Cell Reports

Article

Mast cell regranulation requires a metabolic switch involving mTORC1 and a glucose-6-phosphate transporter

Graphical abstract

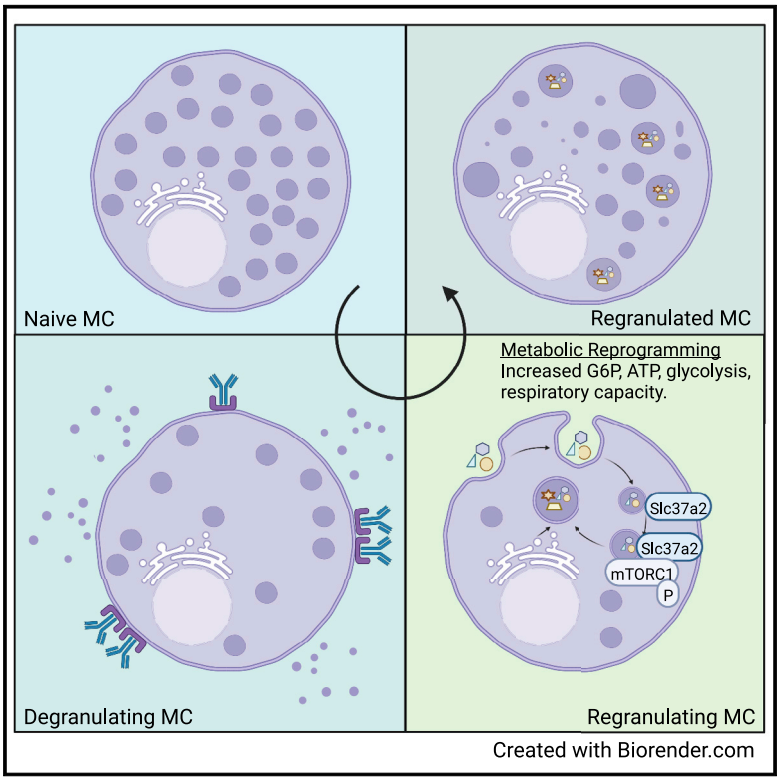

Authors

Jason A. Iskarpatyoti, Jianling Shi, Mathew A. Abraham, Abhay P.S. Rathore, Yuxuan Miao, Soman N. Abraham

Correspondence

soman.abraham@duke.edu

In brief

Mast cells have been shown to have the capacity to reform granules following degranulation *in vitro*. Iskarpatyoti et al. demonstrate that regranulation also occurs *in vivo*. This process requires a metabolic reprogramming that is regulated by an interaction between mTORC1 and the glucose-6-phosphate transporter Slc37a2.

Highlights

- Mast cells can regranulate after each successive anaphylactic reaction in mice
- The interaction of a G6P transporter, Slc37a2, and mTORC1 contributes to regranulation
- Slc37a2 is needed for the metabolic switch regulating regranulation
- Slc37a2 also conveys extracellular medium components into nascent mast cell granules

Iskarpatyoti et al., 2022, Cell Reports *40*, 111346
September 27, 2022
https://doi.org/10.1016/j.celrep.2022.111346

CellPress

Cell Reports

CellPress
OPEN ACCESS

Article

Mast cell regranulation requires a metabolic switch involving mTORC1 and a glucose-6-phosphate transporter

Jason A. Iskarpatyoti,[1] Jianling Shi,[2] Mathew A. Abraham,[2] Abhay P.S. Rathore,[2] Yuxuan Miao,[3] and Soman N. Abraham[1,2,4,5,6,*]

[1]Department of Molecular Genetics & Microbiology, Duke University Medical Center, Durham, NC 27710, USA
[2]Department of Pathology, Duke University Medical Center, Durham, NC 27710, USA
[3]Ben May Department of Cancer Research, The University of Chicago, Chicago, IL 60637, USA
[4]Department of Immunology, Duke University Medical Center, Durham, NC 27710, USA
[5]Program in Emerging Infectious Diseases, Duke-National University of Singapore, Singapore 169857, Singapore
[6]Lead contact
*Correspondence: soman.abraham@duke.edu
https://doi.org/10.1016/j.celrep.2022.111346

SUMMARY

Mast cells (MCs) are granulated cells implicated in inflammatory disorders because of their capacity to degranulate, releasing prestored proinflammatory mediators. As MCs have the unique capacity to reform granules following degranulation *in vitro*, their potential to regranulate *in vivo* is linked to their pathogenesis. It is not known what factors regulate regranulation, let alone if regranulation occurs *in vivo*. We report that mice can undergo multiple bouts of MC regranulation following successive anaphylactic reactions. mTORC1, a nutrient sensor that activates protein and lipid synthesis, is necessary for regranulation. mTORC1 activity is regulated by a glucose-6-phosphate transporter, Slc37a2, which increases intracellular glucose-6-phosphate and ATP during regranulation, two upstream signals of mTOR. Additionally, Slc37a2 concentrates extracellular metabolites within endosomes, which are trafficked into nascent granules. Thus, the metabolic switch associated with MC regranulation is mediated by the interactions of a cellular metabolic sensor and a transporter of extracellular metabolites into MC granules.

INTRODUCTION

Mast cells (MCs) are long-lived, highly granulated tissue resident cells of hematopoietic lineage that are located at the host-environment interface (Gurish and Austen, 2012; Metcalfe et al., 1997). Although a primary physiologic role is promoting immune responses to infectious agents (Marshall, 2004; Abraham and St John, 2010; Urb and Sheppard, 2012), MCs are best known for promoting chronic inflammatory disorders such as urticaria, anaphylaxis, arthritis, and asthma (Theoharides and Kalogeromitros, 2006; Amin, 2012; Boyce, 2003; Yu et al., 2006). Many of the pathogenic contributions of MCs are linked to their capacity to release bioactive mediators that are stored within granules such as lysosomal hydrolases, amines, cytokines, chemokines, proteases, and proteoglycans for sustained periods (Wernersson and Pejler, 2014). These mediators, upon release from extracellular MC granules in a process called degranulation, promote the recruitment of various immune cells from circulation into the tissue (Abraham and St John, 2010). However, when MC release of mediators is excessive or unregulated, significant tissue damage can result.

Since MCs are long-lived cells, having been described to survive *in vivo* for several months (Kiernan, 1979; Padawer, 1974), another MC trait thought to promote its pathogenesis is its unique capacity to regranulate in place following degranulation. Indeed, *in vitro* studies have reported that MC degranulation is accompanied by regranulation (Kobayasi and Asboe-Hansen, 1969; Xiang et al., 2001). This suggests that MCs have the potential to undergo multiple cycles of degranulation and regranulation *in vivo*, thereby markedly enhancing their capacity to contribute to pathologies found in chronic allergic conditions such as asthma or atopic dermatitis, where significant changes to tissue homeostasis are observed (Ando et al., 2013; Okayama et al., 2007). However, at this time, it is not known if multiple cycles of MC degranulation and regranulation can occur *in vivo* and, if so, what factors regulate this activity.

While the functional relevance of MC degranulation is well established, the biogenesis of MC granules remains less well known. Investigations of MC granule biogenesis have been limited to mostly microscopy-based studies, and they have revealed that granule formation is initiated by uniform-sized progranules within MCs that bud off from the *trans*-Golgi (Hammel et al., 1985; Combs, 1966). Thereafter, progranules fuse with each other, forming larger, immature granules that ultimately associate with endosomes that are positive for CD63, a secretory lysosomal membrane marker (Hammel et al., 2010; Moon

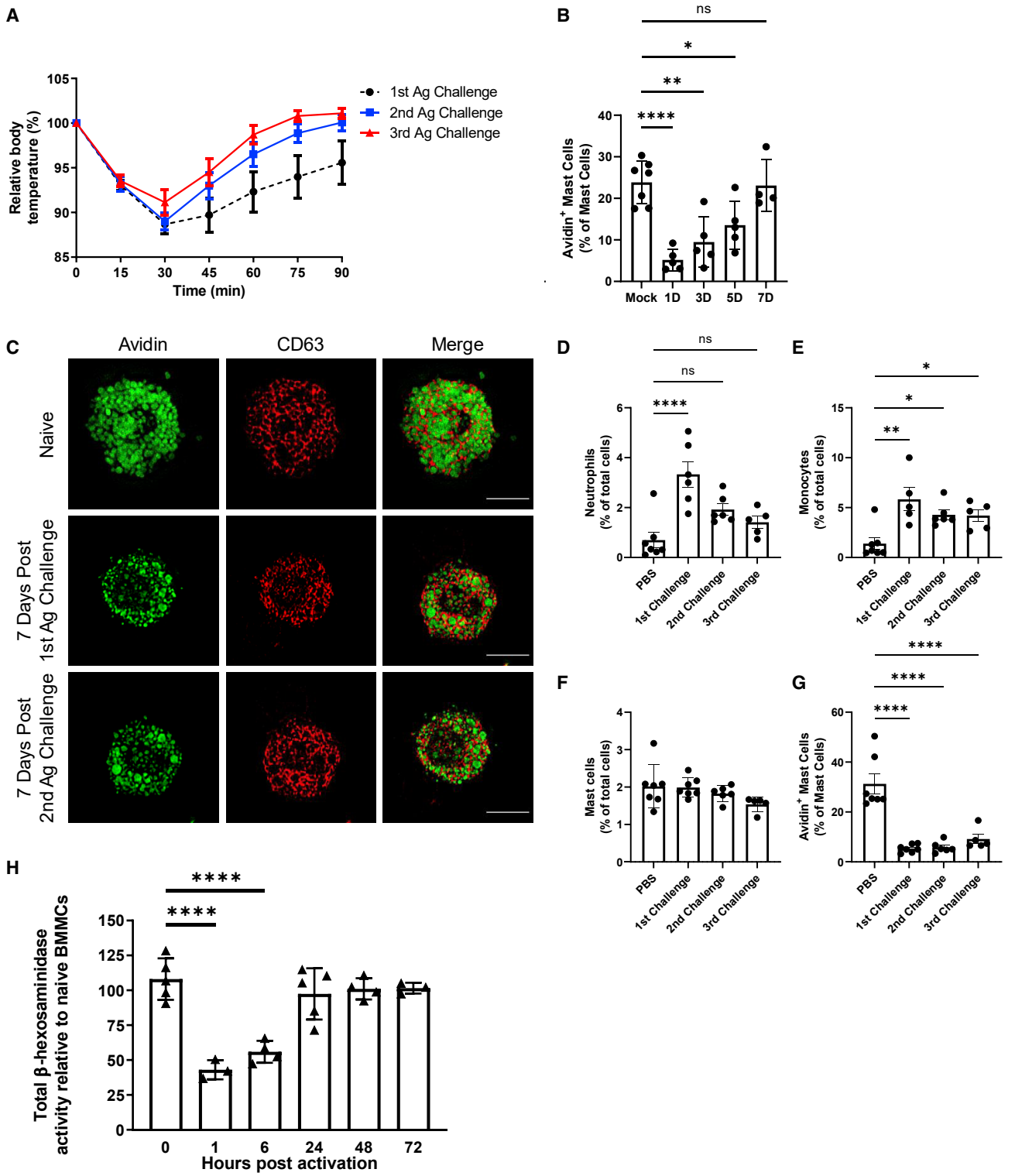

Figure 1. Regranulated MCs are capable of causing repeat anaphylaxis *in vivo*

(A) Core body temperatures following three Ag challenges, each separated by 7 days (n ≥ 7 mice).

(B) Flow cytometry analysis of CD45$^+$cKit$^+$avidin$^+$ MCs in peritoneal lavages at time points indicated post initial Ag challenge (n ≥ 4 mice).

(C) Immunofluorescence images of naive peritoneal MCs or 7 days post Ag challenge a first or second time. Cells are immunostained with avidin (green) and CD63 (red). Images are representative of at least 2 independent experiments. Scale bars represent 10 μm.

(legend continued on next page)

et al., 2014; Azouz et al., 2014). Biochemical studies of isolated MC granules have shown them to contain a dense core comprising of negatively charged serglycin proteoglycans, which avidly bind to positively charged granule components such as chymase and tryptase (Rönnberg et al., 2012). Cumulatively, these ionic interactions stabilize the granule structure and keep the granule components from rapidly disaggregating immediately upon release from MCs, allowing distant communications within the body (Kunder et al., 2009; St John et al., 2012).

Conceivably, mechanisms involved in the initial biogenesis of granules, such as protein and lipid synthesis, intracellular trafficking of progranules and vesicles, and packaging of granule components within MC granules are also involved in MC regranulation. Since the bulk of these activities will require significant energetic demands, we hypothesized that following degranulation, marked metabolic reprogramming within MCs would occur to accommodate regranulation. It is well known that mTOR, an evolutionarily conserved serine/threonine (ser/thr) kinase, is a critical regulator of the metabolic switch that occurs during T cell differentiation (Chi, 2012; Salmond, 2018). Specifically, mTORC1, one of two complexes formed by mTOR, is activated upon sensing sufficient glucose and amino acid levels, which leads to downstream phosphorylation of 4E-BP and S6K, which results in protein and lipid synthesis (Saxton and Sabatini, 2017a). Additionally, mTORC1 activation is required for increased glycolysis in T cells during differentiation (Finlay, 2012). Based on these observations, we propose that mTORC1 activation is necessary for MC regranulation. Here, we sought to validate this notion and as well as identify additional factors in MCs that contribute to MC regranulation.

RESULTS

MCs can undergo multiple bouts of degranulation and regranulation in mice

To date, the capacity of MCs to undergo more than one round of degranulation *in vivo* has not been studied. Here, we investigated if immunoglobulin E (IgE)-sensitized peritoneal MCs can undergo multiple rounds of degranulation *in vivo* following serial exposure to antigen (Ag). A mouse model of anaphylaxis was used to assess the inflammatory response induced by and correlated to the degranulation of IgE sensitized MCs (Ang et al., 2016; Choi et al., 2018). To induce MC degranulation, we passively sensitized mice with TNP-specific IgE intraperitoneally (i.p.), then challenged these mice 16 h later with TNP-OVA Ag i.p. All the sensitized mice experienced anaphylaxis as shown by a drastic drop in core body temperature (Figure 1A, first Ag challenge). We observed that temperatures began to drop in the mice within 15 min of Ag challenge. Temperatures continued to drop for 30 min before returning to baseline core body temperature (Figure 1A).

Since MCs have demonstrated the capacity to regranulate *in vitro* (Xiang et al., 2001; Kobayasi and Asboe-Hansen, 1969), we reasoned that recently degranulated mouse peritoneal MCs should regranulate *in vivo* and participate in additional anaphylactic reactions when rechallenged with Ag. To investigate if recently degranulated MCs could regranulate *in vivo*, we collected peritoneal MCs from mice on days 1, 3, 5, and 7 following anaphylaxis and measured intracellular avidin, a probe for heparin (Tharp et al., 1985) in MCs, to assess granularity. As expected, the percentage of MCs containing high levels of avidin were significantly diminished on day 1, indicating that MCs were degranulated during anaphylaxis (Figure 1B). MCs containing high levels of avidin increased over the 7-day time course, reaching a similar percentage of MCs as naive mice by day 7 (Figure 1B).

To further examine the state of granulation of these MCs, we collected peritoneal cells from mice on day 7 post Ag challenge and compared them with peritoneal cells from naive mice via microscopy. MCs from both groups of mice were stained with anti-CD63 antibody, a probe for MC granule membranes, and avidin-fluorescein isothiocyanate (FITC). In naive mice, avidin-FITC$^+$ and CD63$^+$ MC granules occupied most of the cytoplasm of peritoneal MCs and were of relatively uniform size (Figure 1C, top row). Although the level of granulation in MCs from Ag-challenged mice 7 days prior was comparable to naive MCs, as shown in Figure 1B, the granule size and shape was far more heterogeneous (Figure 1C, middle row). As we would expect newly recruited MCs to appear similar to naive MCs, these results confirm that 7 days after Ag-challenge, MCs are regranulated *in vivo*.

Next, we sought to examine if these regranulated MCs could function regularly by mediating anaphylaxis. A week post initial Ag challenge, we passively sensitized and challenged the same mice again. We found that mice challenged 7 days previously exhibited a comparable drop in core body temperature, reaching the lowest core body temperatures by 30 min (Figure 1A, second Ag challenge). Seven days after the second challenge, peritoneal MCs were examined, and we found that like MCs 7 days after the initial Ag challenge, MC granule size and shape were more heterogeneous than observed in naive mice (Figure 1C, bottom row). Also, a similar drop in body temperature was observed when these mice were sensitized and challenged a third time 7 days later (Figure 1A, third Ag challenge). Interestingly, we observed a trend toward faster recovery time from anaphylaxis after each Ag challenge. These observations reveal that MCs can undergo repeated bouts of degranulation without significant loss in degranulation (or regranulation) capacity.

To further confirm that MCs can undergo multiple bouts of degranulation and regranulation without significant loss in functional capacity, we compared immune cell recruitment into the mouse peritoneal cavity, the site of MC activation, after each

(D–G) Flow cytometry analysis of peritoneal lavages 24 h after the first, second, or third Ag challenge or from PBS-treated control mice. Quantification of these results is shown for (D) CD45$^+$CD11b$^+$Ly6G$^+$ neutrophils, (E) CD45$^+$CD11b$^+$Ly6C$^+$ monocytes, (F) CD45$^+$cKit$^+$ MCs, and (G) CD45$^+$cKit$^+$Avidin^{Hi} intracellular MC staining ($n \geq 6$ mice). See also Figure S1.

(H) Total β-hexosaminidase in BMMCs at time points indicated post activation using ionomycin.

Error bars represent SD (A-B, D-G) and SEM from $n \geq 3$ independent experiments (H). Data were analyzed by a one-way ANOVA with a Tukey's post test (B and D–G) or a one-way ANOVA with a Dunnett's post test comparing each group with untreated BMMC controls (H). *$p < 0.05$; **$p < 0.01$; ***$p < 0.001$; ****$p < 0.0001$; ns, not significant.

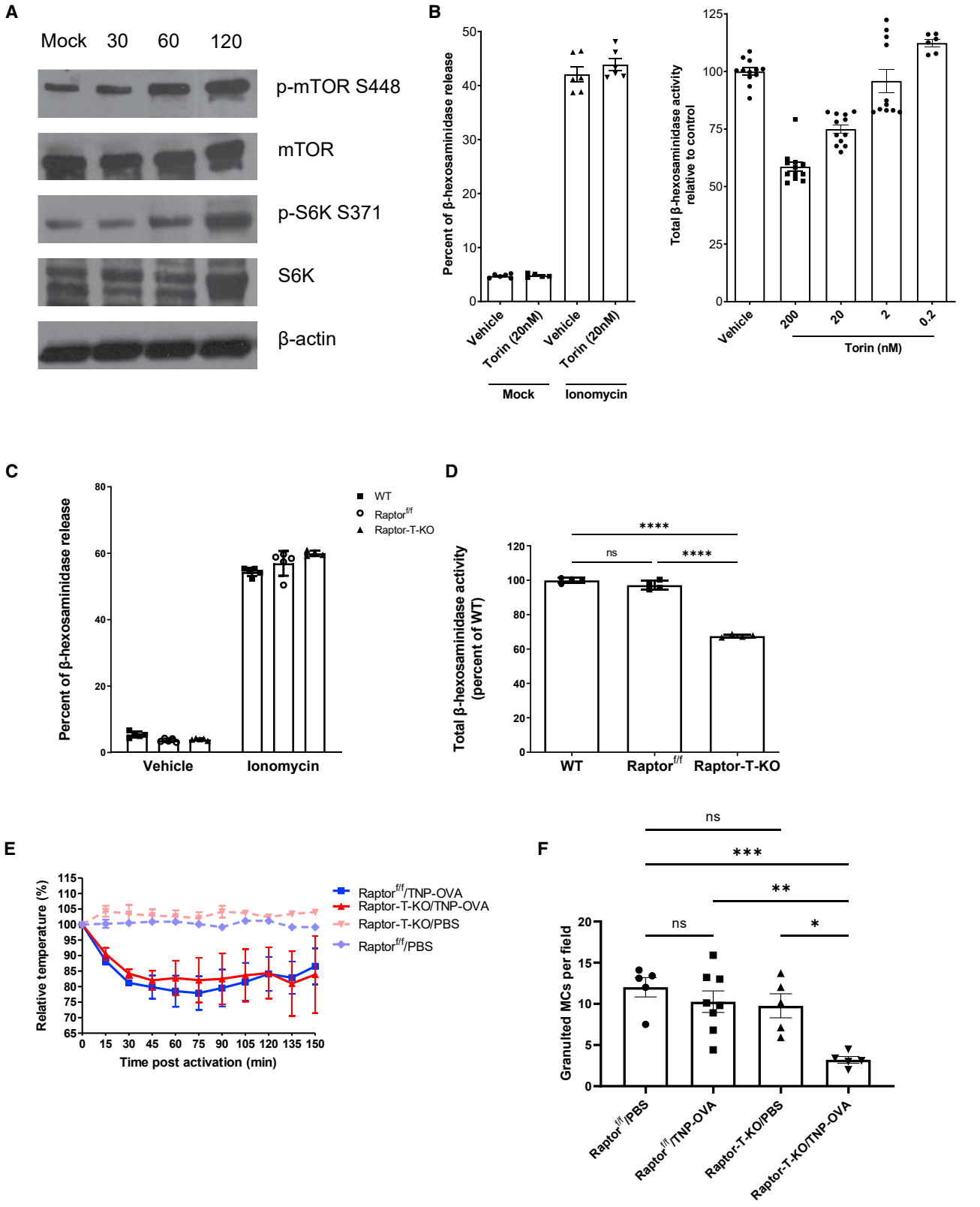

(legend on next page)

Ag challenge. Mice were euthanized 24 h after the first, second, or third Ag challenge, and peritoneal cells were collected by lavage. Inflammatory response was determined by flow cytometry (Figure S1). We found that after the initial Ag challenge, the percentage of $CD45^+CD11b^+Ly6G^+$ neutrophils, and $CD45^+Ly6G^-Ly6C^+$ monocytes, was increased compared with PBS-treated controls (Figures 1D and 1E). Notably, the second and third Ag challenges, while causing anaphylaxis, had a similar percentage of neutrophils in the peritoneum compared with PBS-control mice while maintaining increased monocyte recruitment. Importantly, the percentage of $cKit^+$ MCs in the peritoneum remained similar after each Ag challenge compared with PBS controls (Figure 1F). As expected, intracellular staining with avidin showed that after each Ag challenge, there were significantly fewer $avidin^+$ MCs compared with PBS control mice, suggesting that 24 h after each Ag challenge, MCs were mostly degranulated (Figure 1G). Taken together, this indicates that the second and third Ag challenges resulted in MC degranulation capable of producing robust anaphylaxis inflammatory response.

These findings reveal that MCs have the innate capacity to regranulate *in vivo* after multiple bouts of degranulation, a distinct property that can potentially contribute to sustaining chronic MC mediated inflammatory reactions.

Kinetics of MC regranulation *in vitro*

We sought to elucidate the molecular basis of MC regranulation. First, we investigated the kinetics of MC regranulation. For these studies, we employed cultured primary bone marrow-derived MCs (BMMCs) from mice. To ensure that our studies of MC regranulation were broadly applicable to other modes of MC degranulation, we induced MC degranulation employing ionomycin, a Ca^{2+} ionophore that induces calcium flux, a critical signaling event preceding MC degranulation regardless of the agonist employed. We assessed degranulation and regranulation by measuring residual cellular content of β-hexosaminidase, a component of the granule that is released upon degranulation and is resynthesized within granules when MCs regranulate. As expected, following degranulation, total β-hexosaminidase in BMMCs was significantly reduced compared with untreated controls (Figure 1H). Six h post degranulation, β-hexosaminidase remained largely unchanged; however, between 24 and 48 h post degranulation, BMMCs had recovered β-hexosaminidase comparable to amounts seen prior to degranulation. Thus, *in vitro* MC regranulation takes between 24 and 48 h to complete.

mTORC1 is necessary for MC regranulation

For MCs to fully regranulate, significant protein and lipid synthesis must occur followed by vesicle trafficking and proper packaging of various granule components into granule structures. These processes exert increased metabolic demands on the cell, requiring substantial metabolic reprogramming to increase available energy. A potentially important cellular regulator of metabolic reprogramming is mTOR, a kinase that has been shown to act as a metabolic switch in T cell activation and innate immune cell functions (Chi, 2012; Salmond, 2018; Weichhart et al., 2015). To investigate a possible role for mTOR in MC regranulation, we induced MC degranulation with ionomycin and measured mTOR activity by western blot. We observed that at 2 h post degranulation, mTOR had increased phosphorylation (Figure 2A). Furthermore, S6K, a ser/thr kinase and a downstream target of mTORC1, also appeared to be phosphorylated at the same time point (Figure 2A). To assess the role of mTOR in regranulation, BMMCs were treated with torin, a selective inhibitor of mTOR activation (Liu et al., 2012), prior to degranulation with ionomycin. Torin-pretreated BMMCs exhibited no significant difference in total percentage of release of β-hexosaminidase upon degranulation (Figure 2B, left). However, BMMCs maintained in torin following degranulation demonstrated a dose-dependent inhibition in their capacity to regranulate based on the reduced amounts of total β-hexosaminidase found in BMMCs 48 h post degranulation (Figure 2B, right). This suggests that although mTORC1 plays no significant role in MC degranulation, its activation is necessary for MC regranulation.

To extend these findings, we investigated tamoxifen-inducible regulatory-associated protein of mTOR (Raptor) knockout ($Raptor^{f/f}$ endoplasmic reticulum [ER]-Cre [Raptor-T-KO]) mice. Raptor is a necessary component for the formation of mTORC1. We hypothesized that we could demonstrate the role of mTORC1 by selectively inhibiting MC regranulation without inhibiting the initial granule biogenesis by treating BMMCs derived from these mice with tamoxifen only after granule maturation has

Figure 2. mTORC1 is necessary for MC regranulation *in vitro* and *in vivo*

(A) Western blots of p-mTOR S2448, mTOR, p-S6K S371, S6K, and β-actin at time points indicated post activation by ionomycin. Two independent experiments were performed with similar results.

(B, left) Percentage of β-hexosaminidase release of BMMCs pretreated with torin or DMSO (vehicle control) and then activated by ionomycin in Tyrode's buffer or treated with Tyrode's buffer alone (mock) for 1 h. β-hexosaminidase release was measured and expressed as a percentage of the total. (B, right) Total β-hexosaminidase at 48 h in BMMCs treated with indicated concentrations of torin or DMSO (vehicle) 1 h post activation by ionomycin in Tyrode's buffer. Results are displayed as a percentage of vehicle control ($n \geq 6$ replicates). Three independent experiments were performed with similar results.

(C) Percentage of β-hexosaminidase release of BMMCs from C57BL/6J mice (WT), $Raptor^{f/f}$, or Raptor-T-KO after activation by ionomycin in Tyrode's buffer or Tyrode's buffer alone (vehicle control) for 1 h. β-hexosaminidase release was measured and expressed as a percentage of total ($n \geq 5$ replicates). Data are representative of three independent experiments.

(D) Total β-hexosaminidase in BMMCs from C57BL/6J (WT), $Raptor^{f/f}$, or Raptor-T-KO 48 h post activation by ionomycin in Tyrode's buffer. Results are normalized to WT BMMCs ($n \geq 5$ replicates). Data are representative of three independent experiments. See also Figure S2A.

(E) Core body temperatures of $Raptor^{f/f}$ or Raptor-T-KO mice following antigen challenge. Results are expressed as relative body temperature compared to initial temperatures ($n \geq 5$ mice).

(F) Total number of toluidine blue stained cells (granulated MCs) in peritoneal lavages of C57BL/6J (WT), $Raptor^{f/f}$, and Raptor-T-KO mice 7 days post Ag challenge. Granulated MCs were counted in ten fields of focus per mouse. See also Figures S2B and S2C.

Error bars represent SD (B-E) and SEM from $n \geq 5$ mice (F). Data were analyzed by a Student's t test (B) or a one-way ANOVA with a Tukey's post test (C–F). $^*p < 0.05$; $^{**}p < 0.01$; $^{***}p < 0.001$.

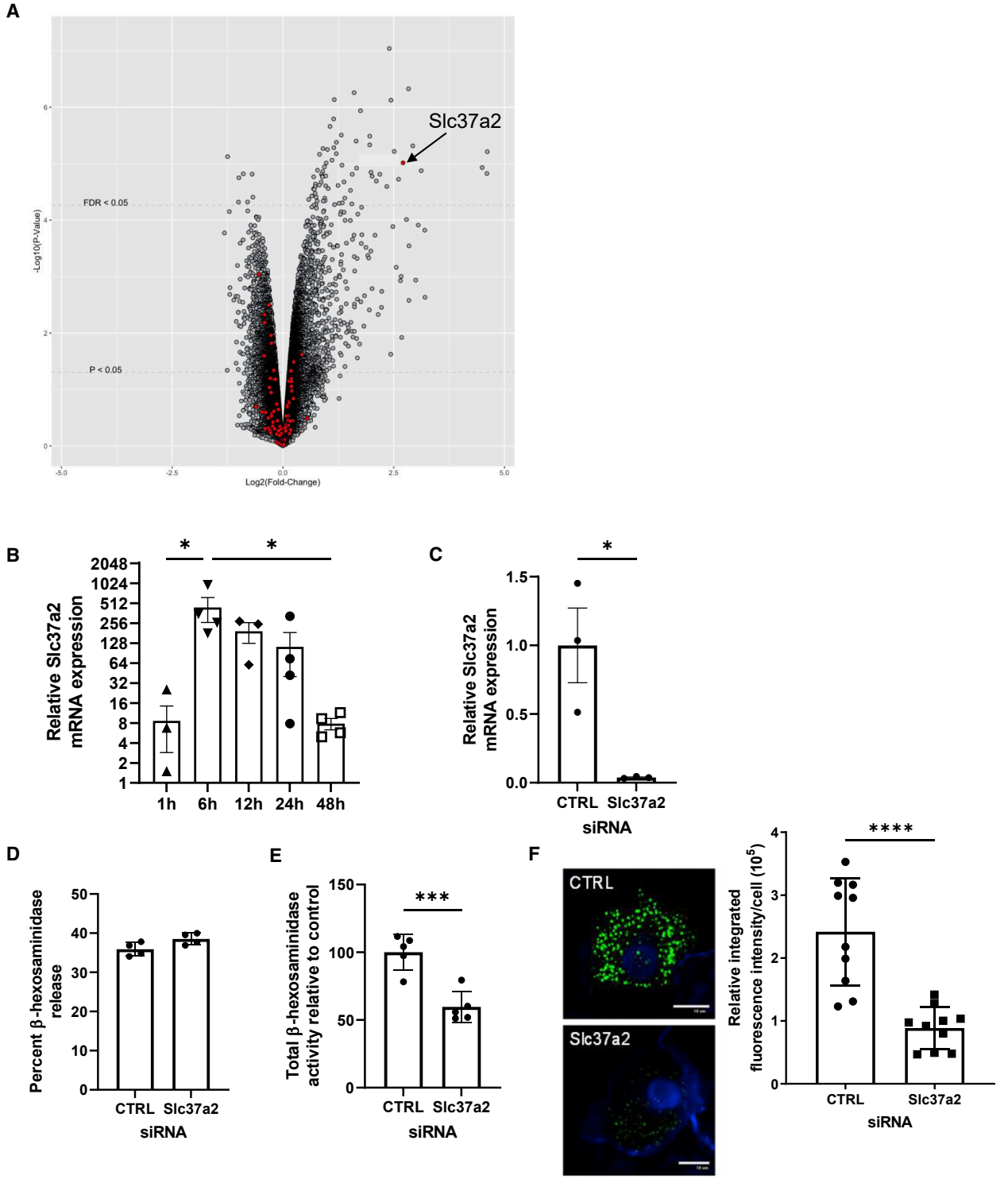

Figure 3. Slc37a2 is a necessary gene in MC regranulation

(A) Volcano plot of microarray analysis of total RNA from three independent samples of naive BMMCs and BMMCs 4 h after activation by ionomycin. Genes with a GO Term of glucose metabolism pathway are highlighted in red.

(B) qRT-PCR analysis of Slc37a2 mRNA in BMMCs at time points indicated post activation with ionomycin. Results are normalized to untreated BMMCs. Error bars represent SEM from n ≥ 3 independent experiments.

(legend continued on next page)

been completed. Mature BMMCs from Raptor-T-KO mice were treated with 4-hydroxytamoxifen to knock out Raptor (Figure S2A). Raptor KO was confirmed by western blot (Figure S2B). We found that upon degranulation with ionomycin, tamoxifen-treated Raptor-T-KO BMMCs contained a similar amount of β-hexosaminidase compared with littermate control (Raptor$^{f/f}$) BMMCs and wild-type (WT) C57BL/6J BMMCs (Figure 2C). Importantly, 48 h after degranulation, Raptor-T-KO BMMCs contained significantly reduced amount of β-hexosaminidase compared with Raptor$^{f/f}$ and WT BMMCs, confirming that mTORC1 is necessary for MC regranulation but not for degranulation (Figure 2D).

To replicate these findings *in vivo*, Raptor-T-KO mice were treated with tamoxifen, and KO was confirmed by PCR (Figure S2C). We then passively sensitized Raptor-T-KO mice and littermate controls with anti-TNP IgE and Ag challenged these mice with TNP-OVA. We found that there was no significant difference in core body temperature drop between Raptor-T-KO mice and littermate controls, suggesting that Raptor-T-KO mice maintain the capacity to undergo MC degranulation and anaphylaxis *in vivo* (Figure 2E). Seven days after Ag challenge, peritoneal cells were collected, and granulated MCs were counted by toluidine blue staining. Compared with littermate controls, PBS-treated Raptor-T-KO mice had similar levels of granulated MCs (Figure 2F), while Raptor-T-KO mice that were Ag challenged had a significantly reduced number of granulated MCs. These results reveal that in Raptor-T-KO mice, the capacity of MCs to undergo regranulation is impaired. Taken together, our findings confirm that the well-known nutrient sensor mTORC1 is necessary for both *in vitro* and *in vivo* MC regranulation.

Slc37a2 is upregulated and necessary for MC regranulation

Having identified mTORC1 as a vital regulator of MC regranulation, we sought to identify the basis of this regulation. Our strategy involved using an unbiased approach to look for highly upregulated metabolic genes following MC degranulation and seeing if they interacted with mTORC1. We examined RNA expression in BMMCs 4 h after ionomycin induced degranulation to selectively identify genes involved in early metabolic activity relating to regranulation while avoiding genes activated during degranulation. From our microarray analysis, we identified 44 genes that were differentially regulated in ionomycin-treated BMMCs compared with naive BMMCs, with an adjusted p value less than 0.05 and at least a 2-fold change (Figure 3A). Among those genes, Slc37a2 stood out as a gene involved in glucose metabolism, a process regulated by mTOR activation (Figure 3A). This gene is part of the Slc37 family of genes that exhibit sequence homology to the bacterial organophosphate/phosphate (Pi) antiporter (Cappello et al., 2018). Slc37a2 has been shown to have the capacity to transport glucose-6-phosphate (G6P) across membranes (Pan et al., 2011) and is involved in regulating glycolysis in macrophages (Wang et al., 2020).

We performed qRT-PCR mRNA analysis of Slc37a2 expression over a 48-h time course following degranulation and revealed expression peaks at 6 h post degranulation, displaying a >400-fold increase in mRNA. Thereafter, expression begins to subside, decreasing significantly and approaching baseline by 48 h (Figure 3B).

To determine if Slc37a2 contributes to MC regranulation, we knocked down its expression in BMMCs using small interfering RNAs (siRNAs). As shown in Figure 3C, Slc37a2 mRNA in BMMCs was markedly reduced compared with control siRNA-treated BMMCs. Furthermore, when we degranulated these Slc37a2-knocked down BMMCs, no significant impairment in β-hexosaminidase release was seen compared with control siRNA treated BMMCs (Figure 3D). Notably, 48 h after degranulation, Slc37a2-downregulated BMMCs had significantly impaired regranulation compared with controls (Figure 3E). Furthermore, when we sought to visualize granules 48 h after degranulation in siRNA-treated BMMCs using an antibody to the granule component serotonin as a probe, we found that in contrast to control BMMCs, very few serotonin granules were observed in Slc37a2-downregulated BMMCs (Figure 3F, left), and there was a significant reduction in the relative integrated fluorescence intensity per cells (Figure 3F, right). Taken together, these findings reveal that Slc37a2 is necessary for MC regranulation.

Slc37a2 concentrates extracellular medium contents acquired by fluid phase endocytosis in endosomes

To deduce the role of Slc37a2 in MC regranulation, we first sought to visualize Slc37a2 localization in relation to their granules throughout the early stages of regranulation. For these studies, we utilized mouse peritoneal MCs, which are markedly more granulated than cultured BMMCs (Malbec et al., 2007). Remarkably, in naive MCs, Slc37a2 appeared to localize within MC granules that were encased in CD63^{+} granule membranes (Figure 4A, top row), indicating that it was a regular MC granule component. As expected, 1 h post degranulation, MCs appeared fully degranulated, as no avidin-FITC staining residual granules were detected (Figure 4A, middle row). Consistent with this finding, most of the CD63^{+} membranes appeared to be localized at the cell periphery (Schäfer et al., 2010). These cells also appeared to stain poorly for Slc37a2, indicating that

(C) qRT-PCR analysis of Slc37a2 mRNA in Slc37a2 siRNA-treated BMMCs compared with control siRNA (CTRL)-treated BMMCs. Results were normalized to control siRNA-treated BMMCs. Error bars represent SEM from n ≥ 3 independent experiments.
(D) Percentage of β-hexosaminidase release of siRNA-treated BMMCs compared with control siRNA-treated BMMCs after activation with ionomycin for 1 h. Results were expressed as a percentage of total β-hexosaminidase (n ≥ 4 replicates). Data are representative of three independent experiments. Error bars represent SD.
(E) Total β-hexosaminidase Slc37a2 siRNA-treated BMMCs compared with control siRNA-treated BMMCs 48 h post activation with ionomycin. Results were normalized to control siRNA-treated BMMCs (n > 4 replicates). Data are representative of three independent experiments. Error bars represent SD.
(F) Immunofluorescence images of Slc37a2 siRNA-treated BMMCs compared with control siRNA-treated BMMCs 48 h post activation with ionomycin. Cells are immunostained with serotonin (green) and phalloidin (blue). Scale bars: 10 μm. Serotonin was quantified using ImageJ (n ≥ 10 cells). Error bars respresent SD.
Data were analyzed by a one-way ANOVA with a Tukey's post test (B) or a Student's t test (C–F). *p < 0.05; **p < 0.01; ***p < 0.001; ****p < 0.0001.

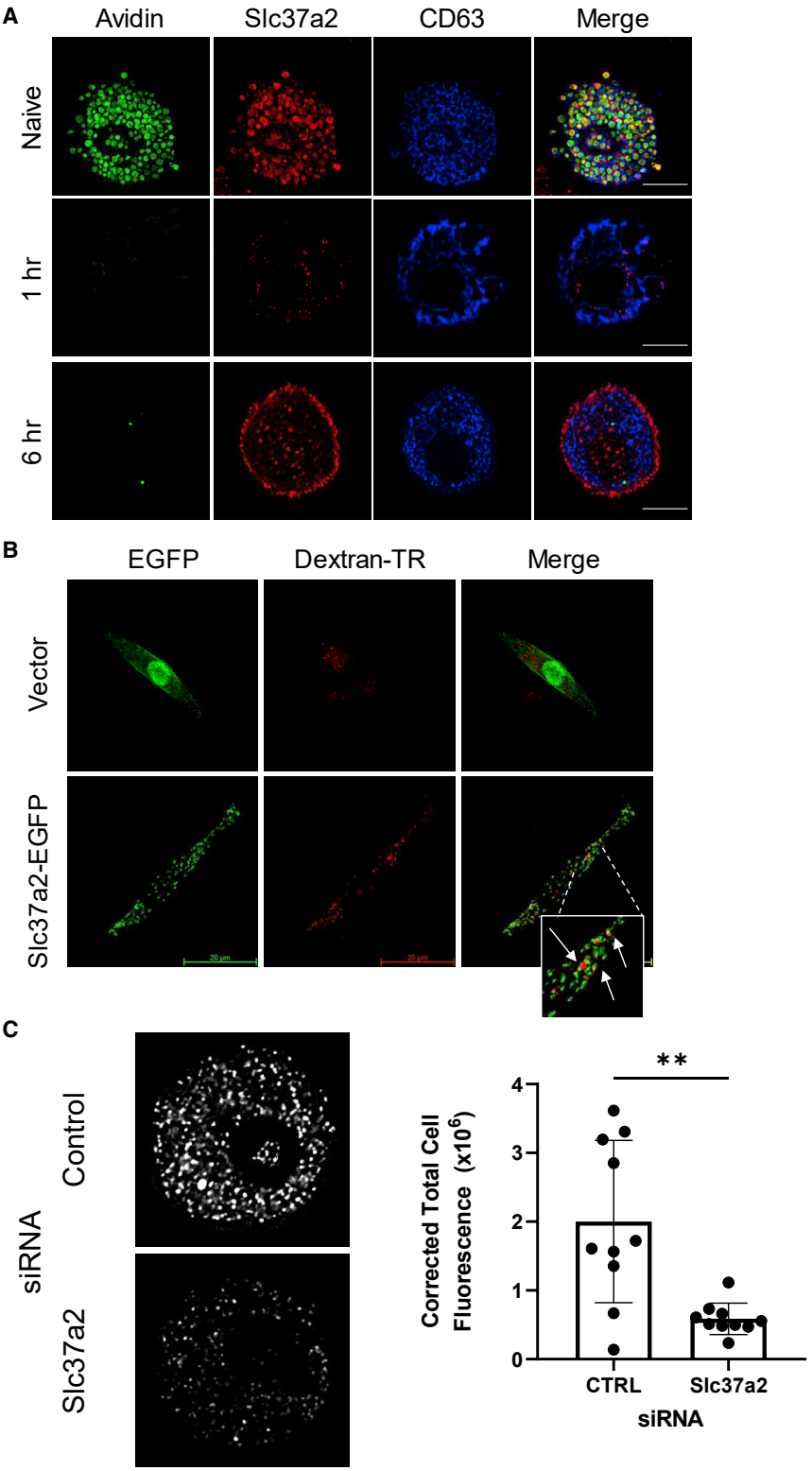

Figure 4. Slc37a2 localizes to endosomes during MC regranulation, where it concentrates dextran

(A) Immunofluorescence images of peritoneal MCs at time points indicated post activation with ionomycin. Cells are immunostained with avidin (green), Slc37a2 (red), and CD63 (blue). Scale bars: 10 μm.

(B) Immunofluorescence images of Slc37a2-EGFP or EGFP vector expressing (green) RBLs incubated with Texas red dextran (red) overnight. Arrows indicate Texas red dextran found within Slc37a2^{+} vesicles. All images are representative of at least 2 independent experiments.

(C) Immunofluorescence images of Slc37a2 siRNA- or control siRNA-treated BMMCs incubated overnight with Texas red dextran (gray). Texas red dextran was quantified using ImageJ ($n \geq 10$ images). Error bars represent SD.

Data were analyzed using a Student's t test. $^{**}p < 0.01$.

the cellular content of Slc37a2 was markedly reduced with the exteriorization of MC granules. However, at 6 h post degranulation, which corresponded to the peak of Slc37a2 expression (Figure 3B), newly formed Slc37a2 appeared localized to the periphery of the cell. Notably, this protein was not associated with $CD63^+$ granule membranes (Figure 4A, bottom row), suggesting that it had a function independent of the mature MC granule. In a previous study, Slc37a2 was shown to concentrate extracellular material taken up by fluid phase endocytosis into endosomes (Kim et al., 2007). To see if Slc37a2 plays a similar role in MCs, we stably over-expressed Slc37a2-EGFP in an immortalized rat MC line, RBL-2H3. We incubated 10,000 MW Texas Red dextran with unstimulated Slc37a2-EGFP expressing RBL-2H3 and found that dextran was concentrated within distinct $Slc37a2^+$ endosomes in MCs (Figure 4B). To extend these findings, we knocked down expression of Slc37a2 in BMMCs using siRNAs and then incubated them with Texas red dextran overnight. We visualized intracellular dextran and found that in Slc37a2-knocked down BMMCs, there was significantly less internalized dextran compared with control siRNA-treated cells (Figure 4C). These data reveal that following MC degranulation, recently produced Slc37a2 concentrates extracellular dextran and potentially other extracellular nutrients in endosomes.

Peripherally located Slc37a2 associates with and activates mTOR

Since both mTORC1 and Slc37a2 are essential for regranulation, we wondered if these MC components interact with each other. In view of our finding that Slc37a2 concentrates extracellular nutrients within endosomes, it is conceivable that this activity may result in mTORC1 activation, analogous to how late endosomes signal to mTORC1 (Flinn et al., 2010). Support for this comes from our finding that at 6 h post degranulation, a subset of mTOR colocalized with nutrient-bearing $Slc37a2^+$ vesicles at the periphery of the MC (Figure 5A). To see if Slc37a2 contributes to mTOR activation, we compared phosphorylation of mTOR following degranulation in control siRNA-treated BMMCs and Slc37a2-knocked down BMMCs. While control siRNA-treated BMMCs displayed increased mTOR phosphorylation by 2 h post degranulation, Slc37a2-knocked down BMMCs exhibited limited mTOR phosphorylation (Figure 5B), suggesting that mTOR phosphorylation requires Slc37a2.

To further support the notion that colocalization of Slc37a2 with mTOR in the cell periphery is critical to mTOR phosphorylation and subsequent MC regranulation, we blocked the trafficking of newly synthesized Slc37a2 to the cell periphery. When BMMCs were treated post degranulation with nocodazole, a microtubule depolymerizer (Vasquez et al., 1997), recently synthesized Slc37a2 accumulated in the perinuclear region of the cell (Figure S3A), whereas in vehicle control-treated BMMCs, Slc37a2 localized as expected to the cell periphery. In contrast to control-treated BMMCs, mTOR in nocodazole-treated BMMCs failed to get phosphorylated (Figure 5C), and these cells regranulated poorly (Figure 5D), indicating that localization of Slc37a2 at the periphery of MCs during regranulation may be critical for mTOR phosphorylation and subsequent regranulation.

Previous studies have shown that G6P signals glucose levels to mTORC1 in cardiomyocytes (Karlstaedt et al., 2020; Roberts et al., 2014). In addition, Slc37a2 has the capacity to transport G6P (Pan et al., 2011). Therefore, we wondered whether Slc37a2 increased intracellular G6P during regranulation to regulate mTOR activation in MCs. To test this, we measured intracellular G6P concentrations in Slc37a2 siRNA-treated BMMCs before degranulation and at 2 and 6 h post degranulation and compared them with control siRNA-treated BMMCs. We found no significant difference in intracellular G6P between Slc37a2 siRNA-treated BMMCs compared with control siRNA-treated cells prior to degranulation. Two h post activation by ionomycin, Slc37a2 siRNA-treated cells trended toward lower G6P concentrations ($p = 0.07$) compared with control siRNA-treated cells. Finally, at 6 h post activation, there was a significantly lower concentration of G6P in Slc37a2 siRNA-treated cells compared with controls (Figure 5E). These results suggest that Slc37a2 is necessary to increase intracellular G6P during regranulation.

Slc37a2 directs metabolic reprogramming linked to MC regranulation

The capacity of Slc37a2 to concentrate nutrients from the extracellular medium into endosomes associated with mTOR, leading to mTOR phosphorylation, suggests that Slc37a2 may play a critical role in regulating MC energy levels to accommodate MC regranulation. Indeed, previous studies have shown that Slc37a2 regulates glycolysis in macrophages (Wang et al., 2020) and the related protein G6PT (Slc37a4) has been shown to be necessary in maintaining G6P, lactate, and ATP amounts in neutrophils (Jun et al., 2014). Since Slc37a2 has the capacity to transport G6P across membranes (Pan et al., 2011), we tested whether blocking G6P metabolism using 2-deoxyglucose (2DG), a glucose analog that cannot be fully metabolized, could inhibit regranulation. We found that treating BMMCs with 2DG 1 h after degranulation significantly reduced MCs' capacity to regranulate (Figure 6A), suggesting that glycolysis is indeed necessary for regranulation.

We next sought to investigate the role Slc37a2 has in glycolysis and oxidative phosphorylation during regranulation. We treated BMMCs with Slc37a2 siRNAs or control siRNAs and performed a mitochondrial stress test prior to degranulation or 6 h after MC degranulation, corresponding to the peak expression of Slc37a2 in WT BMMCs, then we used Seahorse XF to measure extracellular acidification and oxygen consumption rates (Figure 6B). From these experiments we found that basal glycolysis is increased 6 h post degranulation in control siRNA-treated BMMCs, but a corresponding increase in Slc37a2 siRNA-treated cells was not observed (Figure 6C). Additionally, ATP production is increased 6 h post degranulation in control siRNA-treated cells but not in Slc37a2 siRNA-treated cells (Figure 6D). Notably, maximum respiration is significantly increased in control siRNA-treated BMMCs 6 h post degranulation but not in Slc37a2 siRNA-treated BMMCs (Figure 6E).

To demonstrate the importance of Slc37a2 localization on peripheral endosomes to metabolic reprogramming during regranulation, a mitochondrial stress test was performed 6 h post degranulation on nocodazole-treated BMMCs (Figure S3B). We found that both basal respiration and glycolysis were inhibited when Slc37a2 localization was blocked (Figures 6F and

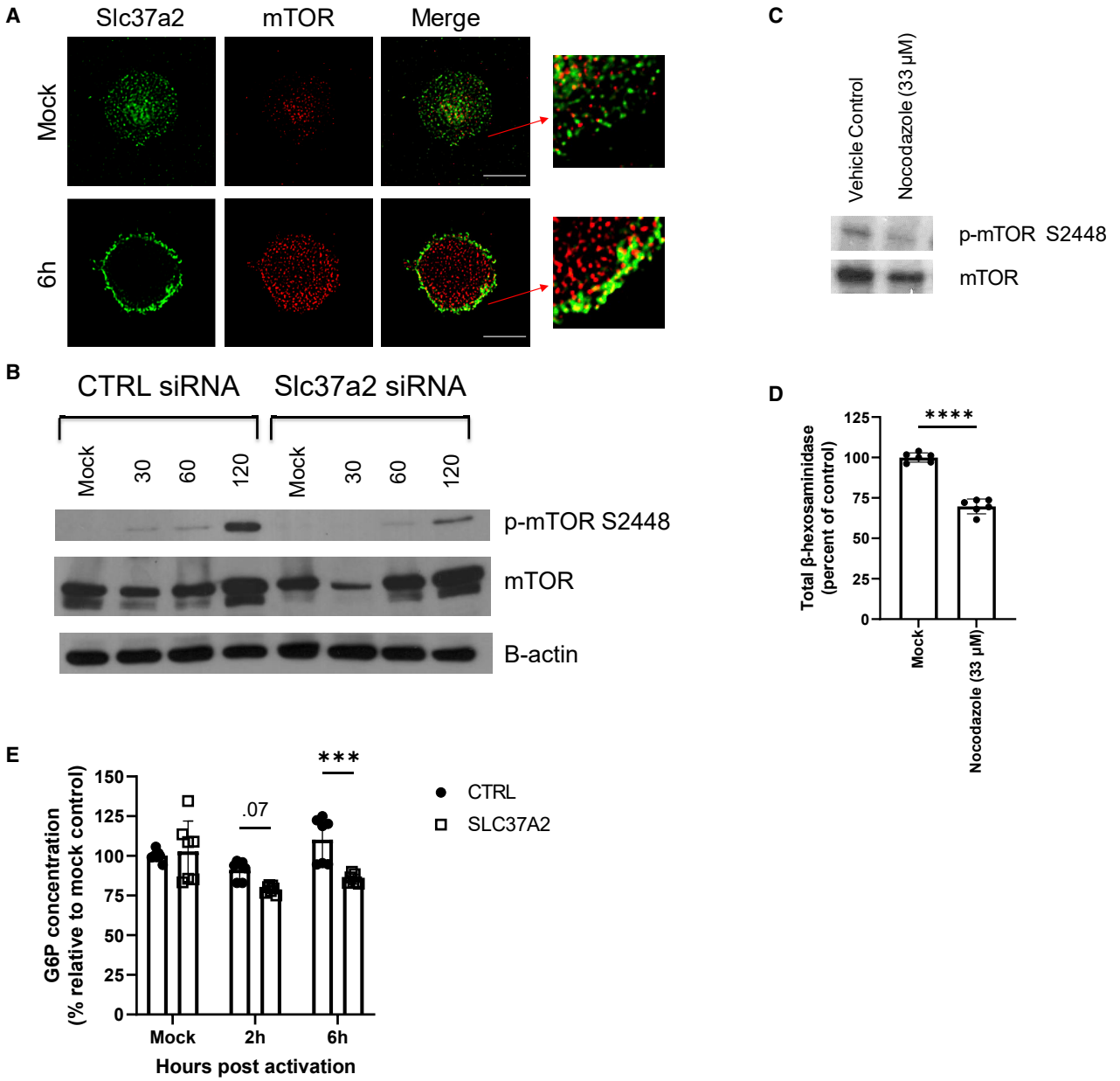

Figure 5. Trafficking of Slc37a2 to endosomes is necessary for mTOR activation

(A) Immunofluorescence images of BMMCs 6 h post activation with ionomycin in Tyrode's buffer or Tyrode's buffer alone (mock). BMMCs were immunostained with Slc37a2 (green) and mTOR (red).

(B) Western blots of p-mTOR S2448, mTOR, and β-actin of Slc37a2 siRNA-treated BMMCs or control siRNA-treated BMMCs at time points indicated. Two independent experiments were performed with similar results.

(C) Western blots of p-mTOR S2448 and mTOR of BMMCs treated for 2 h with nocodazole or vehicle control post activation with ionomycin.

(D) Total β-hexosaminidase at 48 h in BMMCs treatment with nocodazole or vehicle control post activation with ionomycin. Results were normalized to vehicle control ($n \geq 5$ replicates). Data are representative of 3 independent experiments. See also Figure S3A.

(E) G6P concentrations in Slc37a2 siRNA-treated BMMCs or control siRNA-treated BMMCs at time points indicated post activation with ionomycin. Results were normalized to untreated control siRNA BMMCs.

Data were analyzed using a Student's t test (D) or a two-way ANOVA with a Bonferroni post test (E). Error bars represent SD. ***$p < 0.001$, ****$p < 0.0001$.

6G). In addition, ATP production and maximum respiration were significantly reduced (Figures 6H and 6I). These results suggest that the specific localization of Slc37a2 to peripheral endosomes during regranulation is critical for the metabolic reprogramming that occurs during regranulation. Furthermore, the presence of Slc37a2 in the cell periphery is necessary for increases in glycolysis, ATP production, and maximum respiration associated with the metabolic shift linked to MC regranulation.

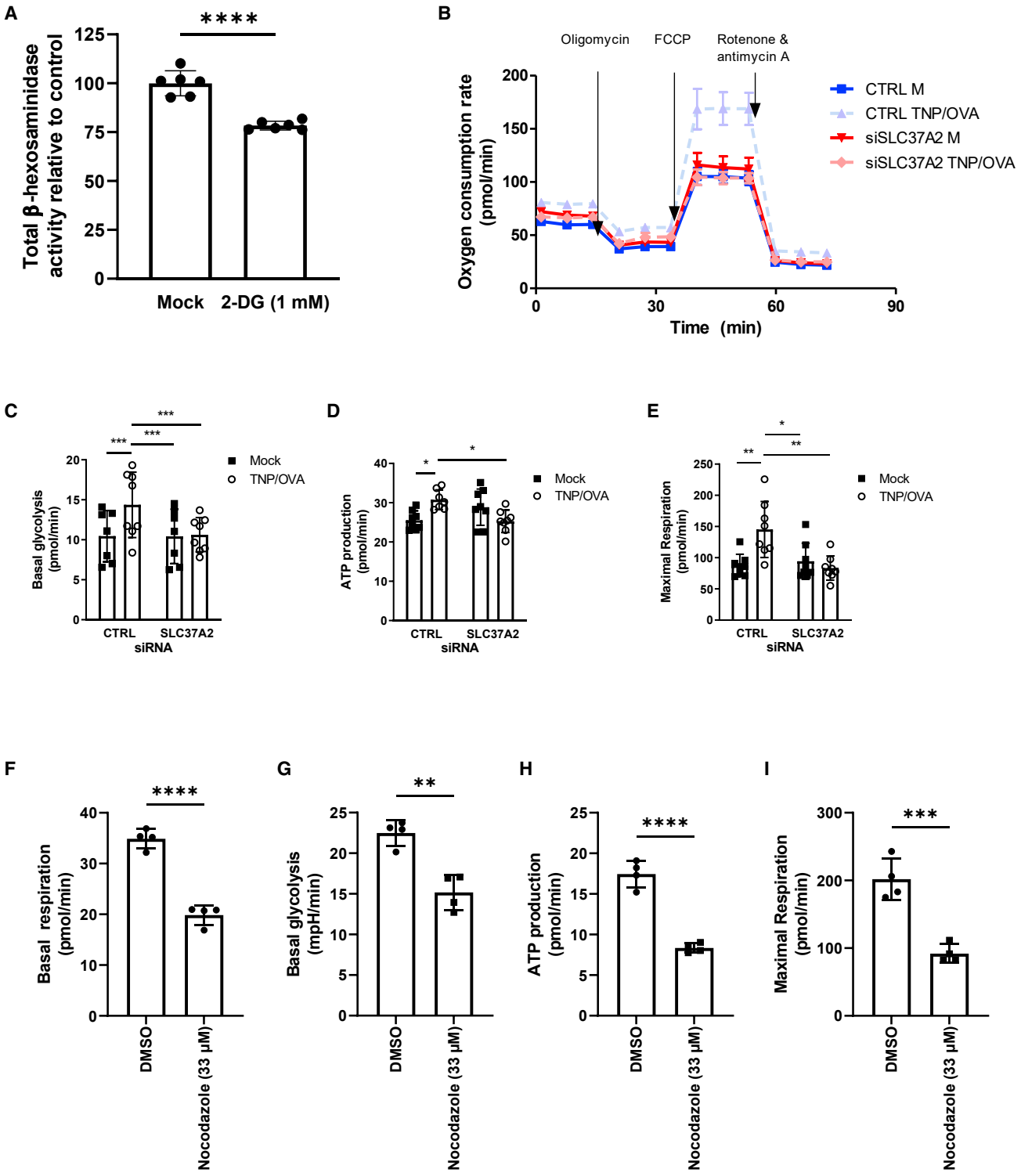

Figure 6. Slc37a2 trafficking to endosomes is necessary for metabolic reprogramming that occurs during MC regranulation

(A) Total β-hexosaminidase at 48 h in BMMC treatment with 2-DG or PBS (mock) post activation with ionomycin. Results were normalized to mock-treated cells (n ≥ 6 replicates). Data are representative of 2 independent experiments.

(B–E) Mitochondrial stress test using the Seahorse XF on Slc37a2 siRNA-treated BMMCs or control siRNA-treated BMMCs 6 h post activation using TNP-specific IgE and TNP/OVA or mock.

(B) Representative Seahorse plot from three independent experiments.

(legend continued on next page)

Slc37a2 conveys components of the extracellular medium into MC granules

Slc37a2 is found within mature MC granules of naive primary MCs (Figure 4A), suggesting that Slc37a2 on the periphery ultimately traffics to and becomes incorporated in nascent MC granules. To investigate if Slc37a2 associates with MC granule contents, we transduced the RBL-2H3 MC line expressing serglycin mCherry to mark and visualize the core of MC granules with plasmids expressing either Slc37a2-EGFP or an EGFP empty vector control. Both sets of transduced serglycin mCherry RBL-2H3 cells were probed for CD63 and visualized by microscopy. As expected, serglycin was localized within CD63-marked vesicles in EGFP empty vector control-transduced RBL-2H3 cells (Figure 7A). Interestingly in Slc37a2 EGFP-expressing RBL-2H3 cells, serglycin appeared encased in Slc37a2$^+$ vesicles with CD63$^+$ membranes seemingly serving to encase granules comprised of serglycin and Slc37a2$^+$ vesicles. Presumably, Slc37a2$^+$ vesicles appeared to have a stronger affinity for MC granules than CD63$^+$-vesicles that typically encase MC granules (Figure 7A). Thus, peripherally located Slc37a2$^+$ vesicles may be destined to become components of MC granules.

If Slc37a2 vesicles are trafficked into MC granules, then cargo acquired from the extracellular medium that is stored and concentrated in these vesicles may also be incorporated into MC granules. To investigate this possibility, we degranulated peritoneal MCs and exposed them to Texas red dextran, a marker of nondescript extracellular medium components. We found that at 48 h, Slc37a2 was associated with nascent avidin$^+$ granules. Furthermore, these granules were also associated with dextran (Figure 7B). This suggests that extracellular components are trafficked in Slc37a2$^+$ endosomes into newly formed granules. To further confirm this, we incubated BMMCs with Texas red dextran for 24 h and then degranulated these BMMCs using ionomycin. We found that a significantly increased amount of dextran was released along with granules compared with unactivated BMMC controls (Figure 7C).

Thus, taken together, Slc37a2 appears to have an additional property of concentrating cargo acquired from the extracellular medium into vesicles that are directly trafficked into MC granules, suggesting that Slc37a2 has the capacity to regulate the composition of MC granules.

DISCUSSION

MCs are best known for their high content of electron-dense secretory granules that occupy most of the cytoplasm of the cell (Wernersson and Pejler, 2014). The capacity of MCs to simultaneously exocytose most of their granules upon activation is one of the primary reasons that MCs are regarded as the early triggers of a wide range of inflammatory disorders such as asthma, arthritis, and anaphylaxis. Although MCs were shown to regranulate *in vitro* over 50 years ago (Kobayasi and Asboe-Hansen, 1969), their capacity to regranulate *in vivo* has remained unclear. Importantly, we found that MCs *in vivo* are capable of regranulating after each successive IgE-mediated activation and that each activation is capable of inducing inflammatory responses comparable to the initial activation of naive MCs. This shows that the regranulation capacity of MCs *in vivo* is comprehensive and restores function. It is noteworthy that *in vivo*, MC regranulation required 7 days to attain granulation levels seen in naive MCs, which is significantly longer than what it takes for BMMCs to regranulate *in vitro*. It is possible that this delay *in vivo* is due to the presence of other inflammatory cells. However, the innate capacity of MCs to undergo at least two rounds of regranulation and degranulation *in vivo* after an initial degranulation response would suggest that in addition to initiating inflammatory responses upon activation, MCs can contribute to sustaining these inflammatory activities for as long as the activating agent is present.

While MCs maintained their capacity to undergo multiple cycles of degranulation and regranulation *in vivo*, changes to the inflammatory response were observed in the second and third MC activation. Our studies were specifically designed to reveal IgE-mediated MC degranulation and to exclude the contribution of other immune cells, such as lymphocytes capable of memory responses. Rather than actively immunizing test mice with OVA Ag, we passively immunized mice with OVA-specific IgE antibodies so that, for the most part, only MCs were sensitized and capable of reacting to each challenge with Ag. Furthermore, Ag challenges of the mice were undertaken 7 days apart, by which time the inflammation induced by the previous challenge had subsided and MCs, which had previously degranulated, had regranulated to similar levels of granule content as naive MCs (Figure 1B). Thus, the immune responses evoked after each challenge were primarily a result of MCs with little or no contribution from innate or adaptive immune cells. Notably, an influx of monocytes was observed after each Ag challenge; however, neutrophil recruitment was reduced in the second and third Ag challenges. This matches the trend toward an increased rate of recovery from anaphylaxis after each subsequent Ag challenge and suggests a possible adaptation of MCs to repeat Ag challenge. Interestingly, a similar observation was made after repeat FcεRI triggering in human cord blood MCs *in vitro* resulted in modulated MC function (Suurmond et al., 2016). It is also notable that 7 days after Ag challenge, regranulated MCs appeared slightly diminished in size (Figure 1C), which may suggest a correlation between MC size and inflammatory response during anaphylaxis. This may be consistent with previous findings that suggest MCs continuously form granules overtime, increasing their granule contents for 6 months or more (Hammel et al., 2010). This would suggest that MCs may increase in size over time when not degranulated.

This capacity of MCs to undergo multiple cycles of degranulation and regranulation is unique. While much is known regarding

(C–E) Basal glycolysis (C), ATP production (D), and maximal respiration (E) were quantified ($n \geq 8$ replicates).
(F–I) Mitochondrial stress test using the Seahorse XF on BMMCs treated with nocodazole post activation with ionomycin. (F) Basal respiration, (G) basal glycolysis, (H) ATP production, and (I) maximal respiration were quantified ($n \geq 4$ replicates). Data are representative from two independent experiments. See also Figure S3B. Data were analyzed by a one-way ANOVA with a Tukey's post test (C–E) or a Student's t test (F–I). Error bars respresent SD. *$p < 0.05$; **$p < 0.01$; ***$p < 0.001$; ****$p < 0.0001$.

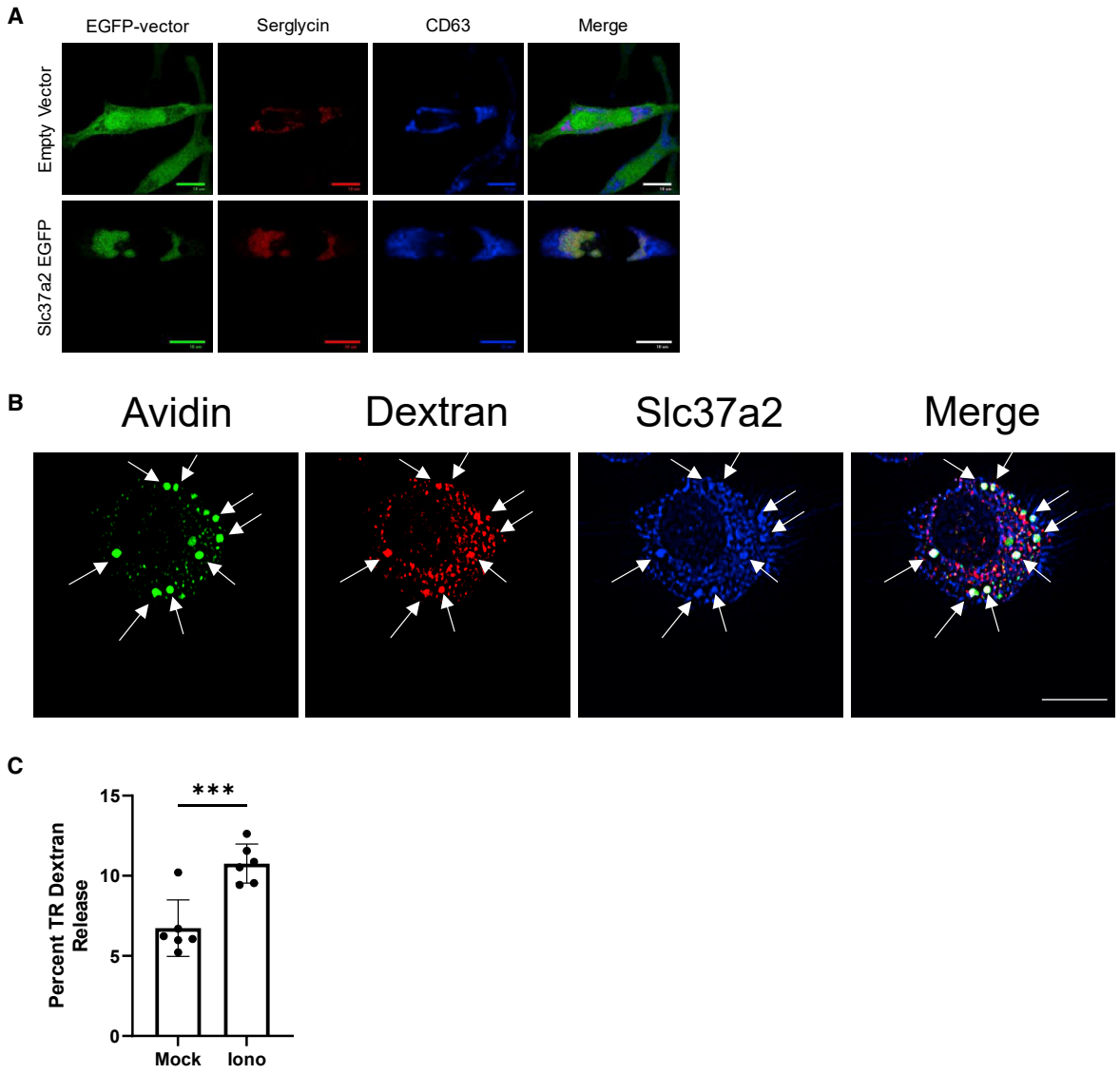

Figure 7. Slc37a2 traffics to nascent granules, carrying dextran into newly formed granules

(A) Immunofluorescence images of RBLs stably expressing serglycin mCherry (red) transduced with lentivirus expressing EGFP or Slc37a2-EGFP (green). Cells were immunostained for CD63 (blue).

(B) Immunofluorescence images of BMMCs incubated for 48 h with Texas red dextran (red) 1 h post activation with ionomycin. BMMCs were immunostained with avidin (green) and Slc37a2 (blue). Arrows indicate colocalization of avidin, dextran, and Slc37a2.

(C) Quantification of Texas red dextran released from BMMCs incubated with Texas red dextran in cell medium overnight and then activated with ionomycin in Tyrode's buffer or in Tyrode's buffer alone (mock) for 1 h. Percentage of released dextran was determined by quantifying the fluorescence signal in supernatant and comparing it to total fluorescence in supernatant and lysed pellet ($n \geq 6$ replicates). Results are representative of two independent experiments.

Data were analyzed using a Student's t test. Erorr bars represent SD. ***$p < 0.001$.

how MCs degranulate and release their granules, comparatively, little is known regarding the molecular events associated with initial MC granule formation, and no information is available on granule reformation. Conceivably, for MCs to fully regenerate the repertoire of granules populating their cytosol, significant protein and lipid synthesis in concert with intracellular vesicle trafficking and packaging of various granule components into the granule structure would need to occur. These activities require significant energy, and so MCs would need to undergo significant metabolic reprogramming. Our studies have implicated the protein kinase mTOR, the well-known mediator of cellular metabolism, growth, and proliferation, as the cellular switch initiating MC regranulation-associated activities (Saxton and Sabatini, 2017b). This conclusion is based on the findings that (1) mTOR and S6K, a ser/thr kinase and a signaling substrate downstream of mTOR, become phosphorylated following MC degranulation, (2) impeding mTOR activation with a chemical inhibitor, torin, prevents MCs from regranulation *in vitro* without

impeding their capacity to degranulate and (3) genetically knocking out Raptor, a necessary gene for mTORC1 expression, blocks the capacity of MCs to regranulate *in vivo* without affecting their capacity to degranulate. Additionally, mTOR activation during MC regranulation was closely linked to increased glycolysis, ATP production, and maximum respiration in MCs (Figure 6). That mTOR is important for MC regranulation following MC degranulation is consistent with previous reports showing that activation of mTOR in MCs inhibited IgE-mediated MC degranulation and cytokine release as well as their capacity to proliferate (Blatt et al., 2012; Rakhmanova et al., 2018). Presumably, activating mTOR triggers a metabolic switch in steady-state MCs to accommodate regranulation, which interferes with both degranulation and MC proliferation activities.

In association with mTOR, we found that Slc37a2 was a critical regulator of MC regranulation. Slc37a2, a transmembrane protein implicated previously in G6P transport in macrophages (Wang et al., 2020), was the most upregulated gene involved in glucose metabolism that we encountered (Figure 3A), increasing 400-fold over baseline by 6 h after MC degranulation (Figure 3B). Furthermore, newly produced Slc37a2 was found to specifically localize at the MC periphery and on vesicles that had recently endocytosed nutrients found in the extracellular medium (Figure 4). MC uptake of labeled extracellular dextran is analogous to findings in Slc37a2 over-expressing COS cells, where dextran from the extracellular medium was found to be harbored within Slc37a2+ endosomes (Kim et al., 2007). Conceivably, peripherally located Slc37a2 contributes to the uptake of nutrients from the extracellular medium. This is supported by our studies showing that nocodazole treatment of BMMCs, which prevents Slc37a2 trafficking to endosomes, reduced basal respiration, basal glycolysis, ATP production, and maximal respiration 6 h post degranulation, similar to what is observed when Slc37a2 is knocked down by siRNAs (Figures 6C–6I).

So how are these extracellular nutrient-encapsulating Slc37a2$^+$ endocytic compartments in MCs connected to mTOR-mediated metabolic switch and MC regranulation? One possibility is that cargo encased in Slc37a2$^+$ endosomes signals mTOR in a manner analogous to how amino acids, glucose, and ATP borne in lysosomes activates the cellular nutrient sensor mTOR found associating with the lysosome surface and triggering a metabolic switch (Saxton and Sabatini, 2017b). Support for this possibility comes from the finding that nutrient-bearing Slc37a2$^+$ endosomes found in the cell periphery appear to associate with mTOR. Furthermore, knockdown of Slc37a2 results in reduced G6P and ATP within MCs during regranulation, two critical signals for mTORC1 activation. Finally, knocking down of Slc37a2 or preventing the trafficking of Slc37a2 to the cell periphery where it colocalizes with mTOR was found to prevent MC regranulation, emphasizing the critical nature of the Slc37a2-mTOR interactions to this activity.

Another intriguing finding was that during MC regranulation, peripherally located Slc37a2$^+$ endosomes travel to nascent MC granules or progranules, which are located in the "progranule zone," to become MC granule components. While we are not able to ascertain its function within the granule, one possibility is that Slc37a2 contributes to concentrating granule components, making it more compact and particulate, a phenomenon sometimes known as condensation (Hammel et al., 2010). This role for SLC37a2 was recently observed when intracellular Slc37a2$^+$ vesicles within microglia were found to exhibit the capacity to concentrate vesicular contents and reduce vesicle volume to a fraction of its original size. Loss of Slc37a2 blocked this vesicular shrinkage, resulting in its expansion and bloating of the cell (Villani et al., 2019).

What drives SLC37a2$^+$ endosomes to traffic into nascent MC granules during regranulation is unclear. When SLC37a2 was over-expressed in RBL-2H3 cells, SLC37a2 rapidly gathered around MC granules and seemed to displace the CD63$^+$ membranes from around granule cores (Figure 7A). Apparently, SLC37a2 has a stronger affinity for the serglycin-rich and negatively charged granule core than CD63$^+$ membranes. It is noteworthy that when SLC37a2$^+$ endosomes fuse with nascent MC granules, they do so bearing cargo endocytosed from the extracellular medium. Indeed, dextran acquired from the extracellular medium by SLC37a2$^+$ vesicles were translocated to nascent MC granules within 48 h of degranulation. Incorporation of dextran in granules was confirmed by the observation that when MCs were activated, dextran was released along with granules. This finding is consistent with previous claims that histamine and tumor necrosis factor (TNF) found in the extracellular medium could be incorporated into MC granules and released when MCs degranulate (Olszewski et al., 2007; Ohtsu et al., 2002). These studies also reveal that Slc37a2 is potentially a key regulator of MC granule composition. Previous studies have reported that mature MC granules are formed when progranules leave the progranule zone near the Golgi and endoplasmic reticulum (ER) and fuse with other progranules, immature granules, endosomes, or lysosomes. Our studies reveal that regranulation also involves the active participation of vesicles recruited from the plasma membrane bearing cargo from the extracellular medium and reveal the critical role of Slc37a2 as a regulator of MC granule content.

Finally, now that we have demonstrated that MCs have the capacity to regranulate *in vivo*, future studies can be designed to assess the specific contribution of the regranulation property to the pathogenesis of MCs in various inflammatory disorders. If this property is deemed to be significant, selectively targeting it may be an efficient way to temper the excessive activities of MCs without impairing its beneficial role in promoting innate and adaptive immune responses to infectious agents and in maintaining homeostasis.

Limitations of the study

While the Raptor-T-KO mice demonstrated the significance of mTORC1 in MC regranulation, the current study does not completely rule out the effect a global KO of Raptor may have on MC regranulation. Additionally, our study was limited to mice and cell lines from mice and rats; therefore, the role Slc37a2 has in human MCs has yet to be demonstrated. Finally, in our microarray study, Slc37a2 isoform 2 was identified; however, the role additional isoforms may have in MC regranulation is unclear.

STAR★METHODS

Detailed methods are provided in the online version of this paper and include the following:

- KEY RESOURCES TABLE

SUPPLEMENTAL INFORMATION

Supplemental information can be found online at https://doi.org/10.1016/j.celrep.2022.111346.

ACKNOWLEDGMENTS

We thank the Duke Cellular Metabolism Analysis Core, especially Amanda Nichols, for their expertise and support on our Seahorse XF experiments. We thank the Duke Microarray Core facility (a Duke NCI Cancer Institute and a Duke Genomic and Computational Biology shared resource facility) for their technical support, microarray data management, and feedback on the generation of the microarray data reported in this manuscript. We would also like to thank the Duke Genomic Analysis and Bioinformatics Core and Dr. David Corcoran for their assistance with analyzing our microarray data. This project was supported by funds from NIH R01-GM144606 and research funds from the Department of Pathology at Duke University.

AUTHOR CONTRIBUTIONS

J.A.I. designed, performed, and analyzed most of the experiments. M.A.A. and J.S. helped perform some of the animal experiments. J.S. also performed the flow cytometry experiments. Y.M. and S.N.A. conceived the project. A.P.S.R. provided technical assistance on flow cytometry data. The manuscript was written by J.A.I. and S.N.A. with helpful comments from A.P.S.R. and Y.M.

DECLARATION OF INTERESTS

The authors declare no competing interests.

Received: November 12, 2021
Revised: June 16, 2022
Accepted: August 22, 2022
Published: September 27, 2022

REFERENCES

Abraham, S.N., and St John, A.L. (2010). Mast cell-orchestrated immunity to pathogens. Nat. Rev. Immunol. *10*, 440–452. https://doi.org/10.1038/nri2782.

Amin, K. (2012). The role of mast cells in allergic inflammation. Respir. Med. *106*, 9–14. https://doi.org/10.1016/j.rmed.2011.09.007.

Ando, T., Matsumoto, K., Namiranian, S., Yamashita, H., Glatthorn, H., Kimura, M., Dolan, B.R., Lee, J.J., Galli, S.J., Kawakami, Y., et al. (2013). Mast cells are required for full expression of allergen/SEB-induced skin inflammation. J. Invest. Dermatol. *133*, 2695–2705. https://doi.org/10.1038/jid.2013.250.

Ang, W.X.G., Church, A.M., Kulis, M., Choi, H.W., Burks, A.W., and Abraham, S.N. (2016). Mast cell desensitization inhibits calcium flux and aberrantly remodels actin. J. Clin. Invest. *126*, 4103–4118. https://doi.org/10.1172/jci87492.

Azouz, N.P., Zur, N., Efergan, A., Ohbayashi, N., Fukuda, M., Amihai, D., Hammel, I., Rothenberg, M.E., and Sagi-Eisenberg, R. (2014). Rab5 is a novel regulator of mast cell secretory granules: impact on size, cargo, and exocytosis. J. Immunol. *192*, 4043–4053. https://doi.org/10.4049/jimmunol.1302196.

Bibi, S., Zhang, Y., Hugonin, C., Mangean, M.D., He, L., Wedeh, G., Launay, J.M., Van Rijn, S., Würdinger, T., Louache, F., and Arock, M. (2016). A new humanized in vivo model of KIT D816V+ advanced systemic mastocytosis monitored using a secreted luciferase. Oncotarget *7*, 82985–83000. https://doi.org/10.18632/oncotarget.12824.

Blatt, K., Herrmann, H., Mirkina, I., Hadzijusufovic, E., Peter, B., Strommer, S., Hoermann, G., Mayerhofer, M., Hoetzenecker, K., Klepetko, W., et al. (2012). The PI3-Kinase/mTOR-Targeting drug NVP-BEZ235 inhibits growth and IgE-dependent activation of human mast cells and basophils. PLoS One *7*, e29925. https://doi.org/10.1371/journal.pone.0029925.

Boyce, J.A. (2003). The role of mast cells in asthma. Prostaglandins Leukot. Essent. Fatty Acids *69*, 195–205. https://doi.org/10.1016/s0952-3278(03)00081-4.

Cappello, A.R., Curcio, R., Lappano, R., Maggiolini, M., and Dolce, V. (2018). The physiopathological role of the exchangers belonging to the SLC37 family. Front. Chem. *6*, 122. https://doi.org/10.3389/fchem.2018.00122.

Carvalho, B.S., and Irizarry, R.A. (2010). A framework for oligonucleotide microarray preprocessing. Bioinformatics *26*, 2363–2367. https://doi.org/10.1093/bioinformatics/btq431.

Chi, H. (2012). Regulation and function of mTOR signalling in T cell fate decisions. Nat. Rev. Immunol. *12*, 325–338. https://doi.org/10.1038/nri3198.

Choi, H.W., Suwanpradid, J., Kim, I.H., Staats, H.F., Haniffa, M., Macleod, A.S., and Abraham, S.N. (2018). Perivascular dendritic cells elicit anaphylaxis by relaying allergens to mast cells via microvesicles. Science *362*, eaao0666. https://doi.org/10.1126/science.aao0666.

Combs, J.W. (1966). Maturation of rat mast cells. An electron microscope study. J. Cell Biol. *31*, 563–575.

Finlay, D.K. (2012). Regulation of glucose metabolism in T cells: new insight into the role of Phosphoinositide 3-kinases. Front. Immunol. *3*, 247. https://doi.org/10.3389/fimmu.2012.00247.

Flinn, R.J., Yan, Y., Goswami, S., Parker, P.J., and Backer, J.M. (2010). The late endosome is essential for mTORC1 signaling. Mol. Biol. Cell *21*, 833–841. https://doi.org/10.1091/mbc.e09-09-0756.

Gentleman, R.C., Carey, V.J., Bates, D.M., Bolstad, B., Dettling, M., Dudoit, S., Ellis, B., Gautier, L., Ge, Y., Gentry, J., et al. (2004). Bioconductor: open software development for computational biology and bioinformatics. Genome Biol. *5*, R80. https://doi.org/10.1186/gb-2004-5-10-r80.

Gurish, M.F., and Austen, K.F. (2012). Developmental origin and functional specialization of mast cell subsets. Immunity *37*, 25–33. https://doi.org/10.1016/j.immuni.2012.07.003.

Hammel, I., Dvorak, A.M., Peters, S.P., Schulman, E.S., Dvorak, H.F., Lichtenstein, L.M., and Galli, S.J. (1985). Differences in the volume distributions of human lung mast cell granules and lipid bodies: evidence that the size of these organelles is regulated by distinct mechanisms. J. Cell Biol. *100*, 1488–1492. https://doi.org/10.1083/jcb.100.5.1488.

Hammel, I., Lagunoff, D., and Galli, S.J. (2010). Regulation of secretory granule size by the precise generation and fusion of unit granules. J. Cell Mol. Med. *14*, 1904–1916. https://doi.org/10.1111/j.1582-4934.2010.01071.x.

Jun, H.S., Weinstein, D.A., Lee, Y.M., Mansfield, B.C., and Chou, J.Y. (2014). Molecular mechanisms of neutrophil dysfunction in glycogen storage disease type Ib. Blood *123*, 2843–2853. https://doi.org/10.1182/blood-2013-05-502435.

Karlstaedt, A., Khanna, R., Thangam, M., and Taegtmeyer, H. (2020). Glucose 6-phosphate accumulates via phosphoglucose isomerase inhibition in heart muscle. Circ. Res. *126*, 60–74. https://doi.org/10.1161/circresaha.119.315180.

Kiernan, J.A. (1979). Production and life span of cutaneous mast cells in young rats. J. Anat. *128*, 225–238.

Kim, J.Y., Tillison, K., Zhou, S., Wu, Y., and Smas, C.M. (2007). The major facilitator superfamily member Slc37a2 is a novel macrophage- specific gene selectively expressed in obese white adipose tissue. Am. J. Physiol. Endocrinol. Metab. *293*, E110–E120. https://doi.org/10.1152/ajpendo.00404.2006.

Kobayasi, T., and Asboe-Hansen, G. (1969). Degranulation and regranulation of human mast cells. An electron microscopic study of the whealing reaction in urticaria pigmentosa. Acta Derm. Venereol. *49*, 369–381.

Korotkevich, G., Sukhov, V., Budin, N., Shpak, B., Artyomov, M.N., and Sergushichev, A. (2021). Fast gene set enrichment analysis. Preprint at bioRxiv. https://doi.org/10.1101/060012.

Kunder, C.A., St John, A.L., Li, G., Leong, K.W., Berwin, B., Staats, H.F., and Abraham, S.N. (2009). Mast cell-derived particles deliver peripheral signals to remote lymph nodes. J. Exp. Med. *206*, 2455–2467. https://doi.org/10.1084/jem.20090805.

Liu, Q., Kang, S.A., Thoreen, C.C., Hur, W., Wang, J., Chang, J.W., Markhard, A., Zhang, J., Sim, T., Sabatini, D.M., and Gray, N.S. (2012). Development of ATP-competitive mTOR inhibitors. Methods Mol. Biol. *821*, 447–460. https://doi.org/10.1007/978-1-61779-430-8_29.

Malbec, O., Roget, K., Schiffer, C., Iannascoli, B., Dumas, A.R., Arock, M., and Daëron, M. (2007). Peritoneal cell-derived mast cells: an in vitro model of mature serosal-type mouse mast cells. J. Immunol. *178*, 6465–6475. https://doi.org/10.4049/jimmunol.178.10.6465.

Marshall, J.S. (2004). Mast-cell responses to pathogens. Nat. Rev. Immunol. *4*, 787–799. https://doi.org/10.1038/nri1460.

Metcalfe, D.D., Baram, D., and Mekori, Y.A. (1997). Mast cells. Physiol. Rev. *77*, 1033–1079. https://doi.org/10.1152/physrev.1997.77.4.1033.

Moon, T.C., Befus, A.D., and Kulka, M. (2014). Mast cell mediators: their differential release and the secretory pathways involved. Front. Immunol. *5*, 569. https://doi.org/10.3389/fimmu.2014.00569.

Mootha, V.K., Lindgren, C.M., Eriksson, K.F., Subramanian, A., Sihag, S., Lehar, J., Puigserver, P., Carlsson, E., Ridderstråle, M., Laurila, E., et al. (2003). PGC-1alpha-responsive genes involved in oxidative phosphorylation are coordinately downregulated in human diabetes. Nat. Genet. *34*, 267–273. https://doi.org/10.1038/ng1180.

Ohtsu, H., Kuramasu, A., Tanaka, S., Terui, T., Hirasawa, N., Hara, M., Makabe-Kobayashi, Y., Yamada, N., Yanai, K., Sakurai, E., et al. (2002). Plasma extravasation induced by dietary supplemented histamine in histamine-free mice. Eur. J. Immunol. *32*, 1698–1708. https://doi.org/10.1002/1521-4141(200206)32:6<1698::Aid-immu1698>3.0.Co;2-7.

Okayama, Y., Ra, C., and Saito, H. (2007). Role of mast cells in airway remodeling. Curr. Opin. Immunol. *19*, 687–693. https://doi.org/10.1016/j.coi.2007.07.018.

Olszewski, M.B., Groot, A.J., Dastych, J., and Knol, E.F. (2007). TNF trafficking to human mast cell granules: mature chain-dependent endocytosis. J. Immunol. *178*, 5701–5709. https://doi.org/10.4049/jimmunol.178.9.5701.

Padawer, J. (1974). Mast cells: extended lifespan and lack of granule turnover under normal in vivo conditions. Exp. Mol. Pathol. *20*, 269–280. https://doi.org/10.1016/0014-4800(74)90059-8.

Pan, C.J., Chen, S.Y., Jun, H.S., Lin, S.R., Mansfield, B.C., and Chou, J.Y. (2011). SLC37A1 and SLC37A2 are phosphate-linked, glucose-6-phosphate antiporters. PLoS One *6*, e23157. https://doi.org/10.1371/journal.pone.0023157.

Rakhmanova, V., Jin, M., and Shin, J. (2018). Inhibition of mast cell function and proliferation by mTOR activator MHY1485. Immune Netw. *18*, e18. https://doi.org/10.4110/in.2018.18.e18.

Ritchie, M.E., Phipson, B., Wu, D., Hu, Y., Law, C.W., Shi, W., and Smyth, G.K. (2015). limma powers differential expression analyses for RNA-sequencing and microarray studies. Nucleic Acids Res. *43*, e47. https://doi.org/10.1093/nar/gkv007.

Roberts, D.J., Tan-Sah, V.P., Ding, E.Y., Smith, J.M., and Miyamoto, S. (2014). Hexokinase-II positively regulates glucose starvation-induced autophagy through TORC1 inhibition. Mol. Cell *53*, 521–533. https://doi.org/10.1016/j.molcel.2013.12.019.

Rönnberg, E., Melo, F.R., and Pejler, G. (2012). Mast cell proteoglycans. J. Histochem. Cytochem. *60*, 950–962. https://doi.org/10.1369/0022155412458927.

Salmond, R.J. (2018). mTOR regulation of glycolytic metabolism in T cells. Front. Cell Dev. Biol. *6*, 122. https://doi.org/10.3389/fcell.2018.00122.

Saxton, R.A., and Sabatini, D.M. (2017a). mTOR signaling in growth, metabolism, and disease. Cell *169*, 361–371. https://doi.org/10.1016/j.cell.2017.03.035.

Saxton, R.A., and Sabatini, D.M. (2017b). mTOR signaling in growth, metabolism, and disease. Cell *168*, 960–976. https://doi.org/10.1016/j.cell.2017.02.004.

Schäfer, T., Starkl, P., Allard, C., Wolf, R.M., and Schweighoffer, T. (2010). A granular variant of CD63 is a regulator of repeated human mast cell degranulation. Allergy *65*, 1242–1255. https://doi.org/10.1111/j.1398-9995.2010.02350.x.

Shin, J., Wang, S., Deng, W., Wu, J., Gao, J., and Zhong, X.P. (2014). Mechanistic target of rapamycin complex 1 is critical for invariant natural killer T-cell development and effector function. Proc Natl Acad Sci U S A *111*, E776–83. https://doi.org/10.1073/pnas.1315435111.

St John, A.L., Chan, C.Y., Staats, H.F., Leong, K.W., and Abraham, S.N. (2012). Synthetic mast-cell granules as adjuvants to promote and polarize immunity in lymph nodes. Nat. Mater. *11*, 250–257. https://doi.org/10.1038/nmat3222.

Suurmond, J., Habets, K.L.L., Tatum, Z., Schonkeren, J.J., Hoen, P.A.C.'t., Huizinga, T.W.J., Laros, J.F.J., Toes, R.E.M., and Kurreeman, F. (2016). Repeated FcepsilonRI triggering reveals modified mast cell function related to chronic allergic responses in tissue. J. Allergy Clin. Immunol. *138*, 869–880. https://doi.org/10.1016/j.jaci.2016.01.017.

Tharp, M.D., Seelig, L.L., Jr., Tigelaar, R.E., and Bergstresser, P.R. (1985). Conjugated avidin binds to mast cell granules. J. Histochem. Cytochem. *33*, 27–32. https://doi.org/10.1177/33.1.2578142.

Theoharides, T.C., and Kalogeromitros, D. (2006). The critical role of mast cells in allergy and inflammation. Ann. N. Y. Acad. Sci. *1088*, 78–99. https://doi.org/10.1196/annals.1366.025.

Urb, M., and Sheppard, D.C. (2012). The role of mast cells in the defence against pathogens. PLoS Pathog. *8*, e1002619. https://doi.org/10.1371/journal.ppat.1002619.

Vasquez, R.J., Howell, B., Yvon, A.M., Wadsworth, P., and Cassimeris, L. (1997). Nanomolar concentrations of nocodazole alter microtubule dynamic instability in vivo and in vitro. Mol. Biol. Cell *8*, 973–985. https://doi.org/10.1091/mbc.8.6.973.

Villani, A., Benjaminsen, J., Moritz, C., Henke, K., Hartmann, J., Norlin, N., Richter, K., Schieber, N.L., Franke, T., Schwab, Y., and Peri, F. (2019). Clearance by microglia depends on packaging of phagosomes into a unique cellular compartment. Dev. Cell *49*, 77–88.e7. https://doi.org/10.1016/j.devcel.2019.02.014.

Wang, Z., Zhao, Q., Nie, Y., Yu, Y., Misra, B.B., Zabalawi, M., Chou, J.W., Key, C.C.C., Molina, A.J., Quinn, M.A., et al. (2020). Solute carrier family 37 member 2 (SLC37A2) negatively regulates murine macrophage inflammation by controlling glycolysis. iScience *23*, 101125. https://doi.org/10.1016/j.isci.2020.101125.

Weichhart, T., Hengstschläger, M., and Linke, M. (2015). Regulation of innate immune cell function by mTOR. Nat. Rev. Immunol. *15*, 599–614. https://doi.org/10.1038/nri3901.

Wernersson, S., and Pejler, G. (2014). Mast cell secretory granules: armed for battle. Nat. Rev. Immunol. *14*, 478–494. https://doi.org/10.1038/nri3690.

Xiang, Z., Block, M., Löfman, C., and Nilsson, G. (2001). IgE-mediated mast cell degranulation and recovery monitored by time-lapse photography. J. Allergy Clin. Immunol. *108*, 116–121.

Yu, M., Tsai, M., Tam, S.Y., Jones, C., Zehnder, J., and Galli, S.J. (2006). Mast cells can promote the development of multiple features of chronic asthma in mice. J. Clin. Invest. *116*, 1633–1641. https://doi.org/10.1172/jci25702.

STAR★METHODS

KEY RESOURCES TABLE

REAGENT or RESOURCE	SOURCE	IDENTIFIER
Antibodies		
Mouse anti-TNP IgE	BD Biosciences	Cat#557079; RRID: AB_479637
Rat anti-CD63	MBL	Cat#D263-3; RRID: AB_1278815
Rabbit anti-Slc37a2	GeneTex	Cat#GTX85198; RRID: AB_10724676
Mouse anti-serotonin	Dako	Cat#M0758; RRID: AB_2122549
Mouse anti-mTOR	EMD Millipore	Cat#05-1592; RRID: AB_1975357
Rabbit anti-mTOR	Cell Signaling	Cat#2983S; RRID: AB_2105622
Rabbit anti-p-mTOR S2448	Cell Signaling	Cat#5536S; RRID: AB_10691552
Rabbit anti-S6K	Cell Signaling	Cat#9202S; RRID: AB_331676
Rabbit anti-p-S6K S371	Cell Signaling	Cat#9208S; RRID: AB_330990
Mouse anti-β-actin	Sigma	Cat#A2228; RRID: AB_476697
Anti-mouse CD16/CD32	BD Biosciences	Cat#553142; RRID: AB_394657
7-AAD	Biolegend	Cat#424404; RRID: AB_2869266
Pacific Blue anti-mouse CD45	Biolegend	Cat#103126; RRID: AB_493535
PE/Cyanine7 anti-mouse CD117	Biolegend	Cat#105813; RRID: AB_313222
BV510 Rat Anti-CD11b	BD Biosciences	Cat#562950; RRID: AB_2737913
Brilliant Violet 650 anti-mouse Ly-6G	BD Biosciences	Cat#127641; RRID: AB_2565881
BD Optibuild BUV395 Rat Anti-Mouse SiglecF	BD Biosciences	Cat#740280; RRID: AB_2740019
Brilliant Violet 785 anti-mouse Ly-6C	Biolegend	Cat#128041; RRID: AB_2565852
APC anti-mouse F4/80	BD Biosciences	Cat#123116; RRID: AB_893481
Avidin-FITC	BD Biosciences	Cat#554057; RRID: AB_10053562
Chemicals, peptides, and recombinant proteins		
Tamoxifen	Tocris	Cat#6342
TNP-Ovalbumin	Biosearch Technologies	Cat#T-5051-10
Recombinant Mouse IL-3	Biolegend	Cat#575508
Neomycin	Sigma	Cat#N1142
Saponin	Sigma	Cat#8047-15-2
Ionomycin	Sigma	Cat#I0634
Triton-100X	Spectrum Chemical	Cat#9036-19-5
p-nitrophenyl-N-acetyl-β-D-glucosaminide	Sigma	Cat#487052
2-deoxyglucose	Sigma	Cat#D3179
Nocodazole	Sigma	Cat#M1404
Torin 1	Tocris	Cat#4247
BD Cytofix/Cytoperm Fixation and Permeabilization Kit	BD Biosciences	Cat#554722
Prolonged Diamond	Invitrogen	Cat#P36970
Paraformaldehyde	Electron Microscopy Sciences	Cat#15710
Protease Inhibitor Cocktail	Sigma	Cat#P8340
Phosphatase Inhibitor Cocktail 2	Sigma	Cat#P5726
Phosphatase Inhibitor Cocktail 3	Sigma	Cat#P0044
Pierce™ Coomassie (Bradford) Protein Assay Kit	ThermoFisher	Cat#23200
SuperSignal™ West Pico PLUS Chemiluminescent Substrate	ThermoFisher	Cat#34578

(*Continued on next page*)

Continued

REAGENT or RESOURCE	SOURCE	IDENTIFIER
Toluidine blue	Millipore Sigma	Cat#TX0875-2
Nucleofector T Kit	Lonza	Cat#VVCA-1002
Dextran Texas Red 10,000 MW	Thermo Fisher	Cat#D1828
Cell-Tak	Millipore Sigma	Cat#CLS354240
Oligomycin	Sigma	Cat#75351
Carbonyl cyanide 4-(trifluormethoxy) phenylhydrazone	Sigma	Cat#C2920
Rotenone	Sigma	Cat#R8875
Antimycin A	Sigma	Cat#A8674
Critical commercial assays		
RNeasy Mini Kit	Qiagen	Cat#74104
Affymetrix Whole Transcriptome Plus Kit	ThermoFisher	Cat#902280
Affymetrix GeneChip Whole Transcriptome Terminal Labeling Kit	ThermoFisher	Cat#900671
GeneChip Mouse Transcriptome Array 1.0	AffyMatrix	Cat#901171
iScript cDNA synthesis kit	BioRad	Cat#1708890
iQ SYBR Green Supermix	BioRad	Cat#1708880
Glucose-6-phosphate Assay Kit	Sigma	Cat#MAK014-1KT
Deposited data		
Microarray Data	This Paper	GEO Accession: GSE207235
Experimental models: Cell lines		
RBL-2H3 cells	ATCC	Cat#CRL-2256
CHO-KL cells	Dr. Michel Arock (Bibi et al., 2016)	N/A
Amphopack-293 cells	BD Biosciences	Cat#C3201-1
Serglycin-mCherry RBL-2H3	Soman Abraham Lab (Ang et al., 2016)	N/A
Experimental models: Organisms/strains		
Mouse: C57BL/6J	Jackson Laboratory	Cat#000664
Mouse: Raptor$^{f/f}$: B6.Cg-Rptor$^{tm1.1Dmsa}$/J	Jackson Laboratory	Cat#013188
Mouse: Raptor$^{f/f}$ ER-Cre	Dr. Xiao Ping Zhong Lab (Shin et al., 2014)	N/A
Oligonucleotides		
Slc37a2 Forward qPCR Primer, 5′-GCTGCTCCCATGATGTTCCT-3′	This Paper	N/A
Slc37a2 Reverse qPCR Primer, 5′-TTGGCGTTACCCTTCAGGCT-3′	This Paper	N/A
B-actin Forward qPCR Primer, 5′-GATTACTGCTCTGGCTCCTAGC-3′	This Paper	N/A
B-actin Reverse qPCR Primer, 5′-GACTCATCGTACTCCTGCTTGC-3′.	This Paper	N/A
Mouse Slc37a2 siGENOME SMARTpool siRNAs	Dharmacon	Cat#M-060760-01-0005
Silencer^{TM} negative control siRNA	Ambion	Cat#AM4611
Recombinant DNA		
plEGFP-C1 plasmid	Clontech	Cat#6058-1
Software and algorithms		
FlowJo v10	FlowJo, LLC	https://www.flowjo.com/solutions/flowjo/downloads
ImageJ	NIH	https://imagej.nih.gov/ij/

(*Continued on next page*)

Continued

REAGENT or RESOURCE	SOURCE	IDENTIFIER
R statistical Program	R Core	https://www.r-project.org/
Bioconductor	https://bioconductor.org	https://bionconductor.org/install
oligo (R Package)	Carvalho and Irizarry, 2010	https://www.bioconductor.org/packages/release/bioc/html/oligo.html
limma (R Package)	Ritchie et al. (2015)	https://bioconductor.org/packages/release/bioc/html/limma.html
Fgsea	Korotkevich et al. (2021)	https://bioconductor.org/packages/release/bioc/html/fgsea.html
StepOne Software v2.3	Applied Biosciences	https://www.thermofisher.com/us/en/home/technical-resources/software-downloads/StepOne-and-StepOnePlus-Real-Time-PCR-System.html
Prism v.9.0.0	GraphPad	https://www.graphpad.com/scientific-software/prism/
Others		
BD Fortessa X-20	BD Biosciences	N/A
Thunder Imager	Leica	N/A
Synergy H1 microplate reader	BioTec	N/A
Agilent 2100 Bioanalyzer G2939A	Agilent Technologies	N/A
Nanodrop 8000 spectrophotometer	Thermo Scientific	N/A
Nucleofector 2b Device	Lonza	Cat#AAB-1001
Seahorse XF96e Analyzer	Agilent	N/A
Affymetrix GeneChip hybridization oven 645	ThermoFisher	Cat#00-0331
Affymetrix GeneChip Fluidics Station 450	ThermoFisher	Cat#00-0079
StepOnePlus Real-Time PCR System	Applied Bioscience	N/A

RESOURCE AVAILABILITY

Lead contact

Further information and requests for resources and reagents should be directed to and will be fulfilled by the lead contact, Soman N. Abraham (soman.abraham@duke.edu).

Materials availability

The cell lines and plasmids generated in this work can be requested from the lead contact with a completed MTA. This study did not generate new unique reagents.

Data and code availability

- Microarray data have been deposited at GEO and are publicly available as of the date of publication. Accession number is listed in the key resources table.
- This paper does not report original code.
- Any additional information required to reanalyze the data reported in this paper is available from the lead contact upon request.

EXPERIMENTAL MODEL AND SUBJECT DETAILS

Mice

Six-to eight-week-old female C57BL/6J and Raptor$^{f/f}$ mice were purchased from The Jackson Laboratory and housed in Duke University animal facilities. Raptor$^{f/f}$-ER Cre mice were generously donated by Dr. Xiao Ping Zhong at Duke University. Six-to twelve-week-old male and female C57BL/6J and Raptor$^{f/f}$ ER-Cre mice were used for our experiments. Cre negative littermates were used as controls. Raptor ER-Cre mice and littermate controls were treated with 2 mg tamoxifen (Tocris) in 100 μL corn oil via gavage on 5 consecutive days. All animal experiments were performed according to approved protocols by the Duke University Institute Animal Care and Use Committee.

Cell lines

BMMCs were derived from femur bone marrow of WT C57BL/6J, Raptor$^{f/f}$-ER Cre, and Raptor$^{f/f}$ Cre-negative littermate controls. Cells were cultured in RPMI-1640 cell media containing 2 mM L-glutamine (ThermoFisher), 10% heat-inactivated fetal bovine serum (FBS, Hyclone), 1 mM nonessential amino acids (ThermoFisher), 25 mM HEPES (ThermoFisher), 1 mM sodium pyruvate (ThermoFisher), 1X Antibiotic-Antimycotic (ThermoFisher), 5 ng/mL recombinant murine IL-3 (R&D Systems, and 5% stem cell factor-containing supernatant from CHO-KL cells for 4–6 weeks until maturation. CHO-KL cells were a gift from M. Arock (Laboratoire de Biologie et Pharmacologie Appliquée, Paris, France). RBL-2H3 cells (ATCC) and transduced RBL-2H3 expressing SDLC37a2-EGFP were cultured in MEM media containing Earl salt's, 2 mM L-glutamine (ThermoFisher), 15% heat-inactivated FBS, and 1 mM sodium pyruvate. Amphopack-293 cells (BD Biosciences) were cultured in DMEM cell media containing 10% heat-inactivated FBS, 2 mM L-glutamine, and 1X Antibiotic-Antimycotic. BMMCs and RBL-2H3 cells were authenticated by flow cytometry employing mast cell markers and transduced RBL-2H3 cells were authenticated by PCR.

METHOD DETAILS

Anaphylaxis experiments

To induce anaphylaxis, mice were sensitized i.p. with 10 μg anti-TNP IgE (BD Biosciences) in 100 μL sterile PBS. Mice were Ag-challenged 16 h later i.p. with 50 μg TNP-OVA (Biosearch Technologies) in 100 μL sterile PBS. Control mice were challenged with sterile PBS. Core body temperatures were monitored using a rectal thermometer immediately prior to Ag-challenge and then every 15 min for up to 3 h. Repeat Ag-challenges were separated by 7 days and mice were resensitized with 10 μg anti-TNP IgE and Ag-challenged 16 h later with 50 μg TNP-OVA.

Flow cytometry analysis

Mice were Ag-challenged one, two, or three times, as described above in Anaphylaxis Experiments. 24 h after the final Ag-challenge, peritoneal cells were collected after lavage with 5 mL cold 10 mM EDTA in PBS. Samples were washed with PBS containing 5 mM EDTA and 3% FBS (FACS Buffer) and then blocked with 1% anti-mouse CD16/CD32 (BD biosciences), 5% normal rat serum and 5% normal mouse serum in FACS buffer for 10 min at RT. Then, surface staining was performed using 7-AAD (Biolegend) and fluorochrome-tagged antibodies to CD45 and CD117 (both from Biolegend), and CD11b, Ly6G, SiglecF, Ly6C, and F4/80 (all from BD Biosciences). Intracellular staining for Avidin (BD Biolegend) was performed using the BD Cytofix/Cytoperm Fixation/Permeabilization Kit and following manufacturer's instructions. Data was collected using BD Fortessa X-20 (BD Biosciences) and analyzed with FlowJo software (TreeStar). The gating strategy used is described in Figure S1.

Immunofluorescence staining and microscopy

For visualization of BMMCs and peritoneal cells, cells were cytospun onto charged glass slides. For RBL-2H3 cells, cells were seeded onto sterilized glass coverslips and allowed to adhere overnight. Cells were then fixed using 4% paraformaldehyde for 20 min at room temperature (RT). Cells were washed in PBS three times and permeabilized in 0.1% saponin (Sigma) and blocked in 1% BSA (USBiological Life Sciences) in PBS for 20 min at RT. Cells were then incubated with 1% anti-CD63 (MBL), 0.5% anti-Slc37a2 (GeneTex), 1% anti-serotonin (Dako), or 1% anti-mTOR (EMD Millipore) overnight at 4°C. The following day, cells were washed in 0.1% saponin and 1% BSA in PBS three times and incubated with 0.25% fluorescent secondary antibodies (Jackson ImmunoResearch) or 0.2% avidin conjugated with FITC (BD Biosciences) for 1 h at RT. Cells were then washed twice with 0.1% saponin and 1% BSA in PBS and twice with PBS. Slides were mounted with ProLong Diamond (Invitrogen). Images were acquired using the Leica Thunder Imager and analyzed by ImageJ.

β-hexosaminidase assay

For BMMC degranulation assays, BMMCs were plated at 1 × 10^5 cells/well in a 96 well V-bottom plate. Cells were washed in Tyrode's buffer (135 mM NaCl, 5 mM KCl, 1.3 mM $CaCl_2$, 1 mM $MgCl_2$, 5.5 mM glucose, 1% BSA, 20 mM HEPES, pH 7.4) and then incubated with 1 μg/mL ionomycin (Sigma) in Tyrode's buffer for 1 h at 37°C. BMMCs in Tyrode's buffer alone were used as a negative control. After incubation, supernatants were collected and cell pellet was lysed in 0.1% Triton-100X (Spectrum Chemical) in Tyrode's buffer. Collected supernatant and lysed pellet were separately incubated with 3.4 mg/mL p-nitrophenyl-N-acetyl-β-D-glucosaminide (NAG, Sigma) in citrate buffer (pH 4.5) for 1 h at 37°C. Reactions were stopped at 1 h with 0.1 M carbonate buffer (pH 10). Colorimetric measurements were performed at 405 nm using a Synergy H1 microplate reader (BioTek). Percent degranulation was determined as percent β-hexosaminidase activity in supernatant compared to total β-hexosaminidase activity in supernatant and pellet.

To measure regranulation, 1 h post-activation with ionomycin, BMMCs were resuspended in BMMC media and incubated at 37°C for 48 h, unless otherwise noted. Total β-hexosaminidase activity was measured by plating 1 × 10^5 cells/well in a 96 well V-bottom plate. BMMCs were washed in Tyrode's buffer then lysed in 0.1% Triton-100X (Spectrum Chemical) in Tyrode's buffer. Total β-hexosaminidase activity in lysed pellet was determined as described above.

For regranulation experiments using 1 mM 2-deoxyglucose (Sigma), 33 μM nocodazole (Sigma), or 20 nM torin (Tocris), BMMCs were treated 1 h post degranulation with each respective inhibitor in BMMC medium. Total β-hexosaminidase activity was measured 48 h post degranulation.

Western Blot

Cells were lysed at indicated time points post degranulation using RIPA buffer (Sigma) supplemented with protease inhibitor cocktail (Sigma) and phosphatase inhibitor cocktails 2 and 3 (Sigma). Lysates were incubated at 4°C for 30 min and supernatants were collected after centrifugation at 20,000xG at 4°C for 15 min. Total protein concentrations were determined using the Pierce™ Coomassie (Bradford) Protein Assay Kit according to manufacturer's instructions (ThermoFisher). Equal concentrations of cell lysates were prepared in Laemmli buffer (BioRad) containing a 5% β-mercaptoethanol (Sigma) and denatured at 95°C for 5 min. Proteins were separated on a 4%–20% mini-PROTEAN TGX precast gel (Biorad) and transferred onto a nitrocellulose membrane by wet transfer. Membranes were blocked in 5% BSA or 5% milk dissolved in TBS (Biorad) containing 0.1% Tween 20 (Sigma) for 45 min and then incubated at 4°C overnight with primary antibodies in blocking buffer. Membranes were washed five times in TBST then incubated with secondary antibody conjugated to horseradish peroxidase (HRP) for 1 h at RT. Membranes were washed five times in TBST then proteins were detected using enhanced chemiluminescent HRP substrate (ThermoFisher). Antibody dilutions were 1:1000 for anti-mTOR, anti-p-mTOR S2448, anti-S6K, and anti-p-S6K S371 (Cell Signaling), and 1:5000 for anti-β-actin (Sigma).

Toluidine blue assay

7 days after mice were Ag-challenged, peritoneal cells were collected after lavage with 5 mL cold 10 mM EDTA in PBS. 100 μLs of cells were cytospun onto glass slides and fixed with Carnoy's fixative (60% ethanol, 30% chloroform, and 10% glacial acetic acid) for 20 min at RT and stained with 0.1% toluidine blue dissolved in PBS containing 0.5N HCl for 20 min. Granulated MCs were visualized and counted under a brightfield microscope.

Microarray

RNA was collected from untreated BMMCs or BMMCs 4 h after treatment with 1 μg/mL ionomycin using the RNeasy Mini Kit. Total RNA was assessed for quality with Agilent 2100 Bioanalyzer G2939A (Agilent Technologies) and Nanodrop 8000 spectrophotometer (Thermo Scientific/Nanodrop). Hybridization targets were prepared with the Affymetrix Whole Transcriptome Plus Kit (Affymetrix) and Affymetrix GeneChip Whole Transcriptome Terminal Labeling Kit (included with Affy Whole Transcriptome Plus) from total RNA, hybridized to GeneChip® Mouse Transcriptome Array 1.0 in Affymetrix GeneChip® hybridization oven 645, washed in Affymetrix GeneChip® Fluidics Station 450 and scanned with Affymetrix GeneChip® Scanner 7G according to standard Affymetrix GeneChip® Hybridization, Wash, and Stain protocols. (Affymetrix, Santa Clara, CA).

Affymetrix Gene Chip microarray data was processed using the *oligo* (Carvalho and Irizarry, 2010) package in the Bioconductor suite (Gentleman et al., 2004) from the R statistical programming environment. Log-scale Robust Multiarray Analysis (RMA) was used to normalize the data and eliminate systematic differences across the arrays. Differential expression between the naive and the wild-type samples was calculated with an empirical Bayes moderated test statistic using the *limma* package (Ritchie et al., 2015). The False Discovery Rate (FDR) was used to control for multiple hypothesis testing. Gene set enrichment analysis (Mootha et al., 2003) (GSEA) was performed using the *fgsea* (Korotkevich et al., 2021) package to identify gene ontology terms and pathways associated with the differentially expressed genes.

RT-qPCR

Total RNA was extracted from BMMCs at indicated time points post ionomycin treatment using the RNeasy mini kit (Qiagen) according to manufacturer's instructions. cDNA was then synthesized using the iScript cDNA synthesis kit (BioRad) and following manufacturer's instruction. Finally, RT-qPCR was performed using iQ SYBR Green Supermix (BioRad) and run on in triplicate on a StepOnePlus Real-Time PCR System (Applied Biosciences) and analyzed by StepOne Software v2.3. mRNA amounts were normalized using β-actin and calculated using the $2^{-\Delta\Delta CT}$ method. The following primer pairs purchased from IDT were used: Slc37a2, 5′-GCTGCTCCCATGATGTTCCT-3′ and 5′-TTGGCGTTACCCTTCAGGCT-3′, β-ACTIN, 5′-GATTACTGCTCTGGCTCCTAGC-3′ and 5′-GACTCATCGTACTCCTGCTTGC-3′.

siRNA treatment

Slc37a2 was knocked down in BMMCs using siGENOME SMARTpool siRNAs (Dharmacon). Transfection of siRNAs into BMMCs was performed using the Amaxa Nucleofector Kit T (Lonza). BMMCs were pelleted and resuspended at a concentration of 2×10^6 cells/100 μL Nucleofector T solution. 300 nM Slc37a2 siRNAs or Silencer™ negative control siRNA (Ambion) was added to the solution. BMMCs were nucleofected using the Amaxa Nucleofector Program U-023. Transfected BMMCs were then resuspended in cell media for 48 h at 37°C prior to assaying.

Dextran uptake assay

RBL-2H3 cells stably expressing Slc37a2-EGFP or EGFP vector control seeded onto coverslips, or BMMCs treated with Slc37a2 siRNAs or negative control siRNAs were incubated with 0.5 mg/mL Dextran Texas Red 10,000 MW in cell media for 16 h at 37°C. Cells were washed twice with cell media and then incubated an additional 2 h in cell media at 37°C. For RBL cells, cells were fixed with 4% paraformaldehyde, washed three times in PBS, and mounted onto a glass slide using Prolong Diamond. For BMMCs, cells were cytospun onto charged glass slides, fixed with 4% paraformaldehyde, washed three times in PBS and then a coverslip was mounted using ProLong Diamond. Images were acquired using the Leica Thunder Imager and analyzed by ImageJ.

Glucose-6-phosphate assay

BMMCs, treated with Slc37a2 siRNA or control siRNA, were activated using 1 μg/mL ionomycin in Tyrode's buffer. 1 h after ionomycin treatment, BMMCs were washed three times and resuspended in BMMC medium. G6P concentrations were determined at 2 h and 6 h post activation and compared to unactivated controls using a G6P kit (Sigma) and following manufacturer's instructions.

Seahorse XF assays

For Slc37a2 siRNA knockdown experiments, Slc37a2 siRNA or control siRNA treated BMMCs were sensitized overnight with 1 μg/mL anti-TNP IgE. Cells were washed three times and resuspended in Tyrode's buffer containing 10 ng/mL TNP-OVA or PBS. After 1 h, cells were washed three times and resuspended in BMMC media. For nocodazole experiments, BMMCs were treated with 1 μg/mL ionomycin or PBS in Tyrode's buffer. 1 h after ionomycin treatment, BMMCs were washed three times and resuspended in BMMC medium containing 33 μM nocodazole. For BMMC adherence, XF96 cell culture microplates were precoated with Cell-Tak following manufacturer's instruction. At 6 h post TNP-OVA or ionomycin treatment, BMMCs were seeded onto Cell-Tak treated XF96 cell culture microplates at a density of 1×10^5 cells/well. Basal oxygen consumption rates (OCR) and extracellular acidification rates (ECAR) were measured using the Seahorse XF96e Analyzer followed by sequential addition of 1 μM oligomycin (Sigma), 0.5 μM carbonyl cyanide 4- (trifluoromethoxy) phenylhydrazone (FCCP, Sigma), and 0.75 μM rotenone (Sigma) with 1.5 μM antimycin A (Sigma). Basal respiration, basal glycolysis, ATP production, and maximal respiration were evaluated based on the manufacturer's instructions.

RBL-2H3 expressing Serglycin-mCherry and Slc37a2-EGFP

RBL-2H3 cells stably expressing serglycin-mCherry were previously generated in our lab (Ang et al., 2016). To generate Slc37a2-EGFP expressing RBLs, Slc37a2 was amplified by PCR from BMMC cDNA and inserted into a plEGFP-C1 plasmid (Takara Bio). Slc37a2 plEGFP-C1 plasmid or plasmid vector control were transfected into Amphopack-293 cells to produce viral particles that were used to infect RBL-2H3 cells or RBL-2H3 cells stably expressing serglycin-mCherry. Slc37a2-EGFP stably expressing cells were selected using neomycin.

QUANTIFICATION AND STATISTICAL ANALYSIS

Statistical analyses were performed using GraphPad Prism v.9.0.0 (GraphPad Software). For comparison between two groups, results were analyzed using a two-tailed unpaired t test. For comparison between multiple groups, results were analyzed using a two-tailed ANOVA with Tukey's post test. A p value less than 0.05 was considered statistically significant. Error bars are represented as SD unless otherwise noted in the figure legend.